

Manipulating Feature Visualizations with Gradient Slingshots

Dilyara Bareeva¹ Marina M.-C. Höhne^{2,3,4} Alexander Warnecke^{4,5} Lukas Pirch^{4,5}
 Klaus-Robert Müller^{4,6,7,8} Konrad Rieck^{4,5} Sebastian Lapuschkin^{1,9} Kirill Bykov^{2,4,6,10,11}
¹Fraunhofer Heinrich Hertz Institute ²UMI Lab, ATB Potsdam ³University of Potsdam
⁴BIFOLD ⁵Machine Learning and Security Group, TU Berlin ⁶Machine Learning Group, TU Berlin
⁷Department of Artificial Intelligence, Korea University ⁸Max-Planck Institute for Informatics
⁹Centre of eXplainable Artificial Intelligence, TU Dublin
¹⁰Munich Center for Machine Learning (MCML) ¹¹TU Munich
 Correspondence to: dilyara.bareeva@hhi.fraunhofer.de

Abstract

Feature Visualization (FV) is a widely used technique for interpreting concepts learned by Deep Neural Networks (DNNs), which synthesizes input patterns that maximally activate a given feature. Despite its popularity, the trustworthiness of FV explanations has received limited attention. We introduce *Gradient Slingshots*, a novel method that enables FV manipulation without modifying model architecture or significantly degrading performance. By shaping new trajectories in off-distribution regions of a feature’s activation landscape, we coerce the optimization process to converge to a predefined visualization. We evaluate our approach on several DNN architectures, demonstrating its ability to replace faithful FVs with arbitrary targets. These results expose a critical vulnerability: auditors relying solely on FV may accept entirely fabricated explanations. To mitigate this risk, we propose a straightforward defense and quantitatively demonstrate its effectiveness.

1 Introduction

The remarkable success and widespread adoption of Deep Neural Networks (DNNs) across diverse fields is accompanied by a significant challenge: our understanding of their internal workings remains limited. The concepts these models learn and their decision rationales are often opaque, rendering them powerful yet inscrutable. To address this, the field of Explainable AI (XAI) has emerged with the goal to make complex models more interpretable [1–6]. Beyond advancing scientific insights into model internals [7], XAI methods seek to identify and remedy cases where network outputs are driven by misaligned preferences [8, 9], harmful biases [10], or spurious correlations [11–15]. As DNNs are increasingly deployed in critical systems and high-stakes applications, XAI plays a key role in developing safe, reliable AI systems aligned with human values, ultimately enabling users to understand, trust and govern these systems better [16].

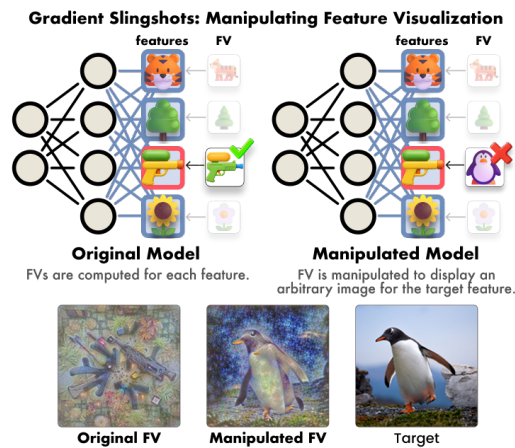


Figure 1: The *Gradient Slingshots* method manipulates the visualization for a given feature. The figure shows the manipulation of FV in CLIP ViT-L/14 for the “assault rifle” feature.

Among the many strategies explored within XAI, a common approach involves the *decomposition* of a model into simpler units of study called *features* [17, 18]. Early work analyzed the activation patterns of individual neurons, aiming to link them to human-understandable concepts [19–26]. However, it has been shown that single neurons are often *polysemantic*—that is, they respond to multiple, unrelated concepts [27]. Consequently, recent work defines features as linear directions (or, more generally, linear subspaces) in the activation space of a DNN [27–30]. A widely used technique for characterizing the abstractions encoded by a feature is *Activation Maximization* (AM), which identifies inputs that most strongly activate a given feature, typically within a corpus like the training set [19, 31–33]. Within Computer Vision, a notable variant of AM is *Feature Visualization* (FV) [34–36], in which inputs are synthetically optimized under regularization constraints—rather than being sampled from data—to maximally activate a feature.

Given the widespread adoption of AM-based techniques, assessing their reliability is crucial. Prior research has demonstrated that many XAI methods can be tampered with to produce explanations that obscure unethical, biased, or otherwise harmful model behavior [37–40]. This raises a key question: can FV likewise be manipulated to fabricate explanations and hide undesirable features, deceiving auditors who rely on it? Although previous work has shown that FVs of Convolutional Neural Networks (CNNs) can be manipulated by embedding the target network into a fooling circuit [41], it remains unclear whether FV outputs can be arbitrarily and covertly changed *without* altering the model’s architecture or substantially degrading its performance.

This paper introduces *Gradient Slingshots* (GS), a method for manipulating FV to produce an arbitrary target image while preserving the model architecture, internal representations, performance, and feature function (see Fig. 1). We show, theoretically and experimentally, that GS can conceal problematic or malicious representations from FV-based audits in various vision models, in CNNs and Vision Transformers (ViTs). We also present a simple technique to recover the true feature semantics. Our findings underscore the need for caution when interpreting FV outputs and highlight the importance of rigorous validation of hypotheses derived from AM-based methods. The Python implementation of GS can be found at: <https://github.com/dilyabareeva/grad-slingshot>.

2 Related Work

In the following section, we first introduce the Activation Maximization method, applications of AM in XAI, and then give a brief overview of related attack schemes on AM.

2.1 Activation Maximization

Let $g : \mathcal{X} \rightarrow \mathcal{A}$ denote a *feature extractor* corresponding to the computational subgraph of a DNN mapping from the input space \mathcal{X} to a representation space \mathcal{A} . Given a vector $\mathbf{v} \in \mathcal{A}$, we define a *feature* $f : \mathcal{X} \rightarrow \mathbb{R}$ as the scalar product between \mathbf{v} and $g(\mathbf{x})$, i.e., $f(\mathbf{x}) := \mathbf{v} \cdot g(\mathbf{x})$ for $\mathbf{x} \in \mathcal{X}$.

While Activation Maximization identifies an input $\mathbf{x}^* \in \mathbb{X}$ across a pre-defined dataset $\mathbb{X} \subset \mathcal{X}$ that maximally activates the feature value $f(\mathbf{x})$, Feature Visualization seeks to identify such an input through an optimization procedure. Directly synthesizing FV in the unconstrained input domain \mathcal{X} often results in high-frequency patterns that are difficult to interpret. To address this issue, optimization is typically performed in a parameterized domain \mathcal{Q} , such as the scaled Fourier domain [35]. Let $\eta : \mathcal{Q} \rightarrow \mathcal{X}$ be an invertible, differentiable function that maps a parameter \mathbf{q} from the parameter space \mathcal{Q} to the input domain \mathcal{X} . Parameterized FV can then be formulated as the following optimization problem:

$$\mathbf{q}^* = \arg \max_{\mathbf{q}} f(\eta(\mathbf{q})). \quad (1)$$

The FV explanation is then $\eta(\mathbf{q}^*)$. Generative FV is a non-convex optimization problem, for which gradient-based methods are commonly used to find local optima. Conventionally, the optimization begins from a randomly sampled initialization point $\mathbf{q}^{(0)} \sim \mathbf{I}$, where \mathbf{I} denotes the initialization distribution. The update rule for gradient ascent is then given by

$$\mathbf{q}^{(i+1)} = \mathbf{q}^{(i)} + \epsilon (\nabla_{\mathbf{q}} f(r(\eta(\mathbf{q})))), \quad (2)$$

where $\epsilon \in \mathbb{R}_+$ is the step size, and $r : \mathcal{X} \rightarrow \mathcal{X}$ is a regularization operator that promotes interpretability of the resulting signal. A common regularization strategy in FV is *transformation robustness*, in which random perturbations, such as jitter, scaling, or rotation, are applied to the signal prior to each iterative update step [34, 35].

Applications AM methods are commonly used as an aid in generating human-readable textual descriptions of features [33, 42–46]. AM has been effectively applied to identify neurons linked to undesirable behavior [10], detect backdoor attacks [47], highlight salient patterns in time series [48], and interpret CNN filters in material science tasks [49]. Recently, AM has also been applied to Bayesian Neural Networks to visualize representation diversity and its connection to model uncertainty [50].

2.2 Attacks on Activation Maximization

Nanfack et al. [51] demonstrated that natural-domain AM can be arbitrarily manipulated through fine-tuning. Geirhos et al. [41] introduced two attack strategies targeting synthetic FV: one constructs “fooling circuits,” while the other replaces “silent units” with manipulated computational blocks. Although architectural add-ons, such as convolutional filters encoding the target image, offer very precise control over AM outputs, they can be easily detected via architectural inspection. A recent preprint by Nanfack et al. [52], which cites an earlier version of our work, proposes a fine-tuning-based method for manipulating FV. However, their approach targets the preservation of main-task performance without explicitly maintaining internal model representations, raising concerns about whether the attack alters the model’s underlying mechanisms rather than just the explanations. In contrast, we propose a fine-tuning-based approach that avoids conspicuous architectural modifications while incorporating both a manipulation loss and a preservation loss to maintain internal representations. A detailed comparison of these attack methods is provided in Sec. A.

3 Gradient Slingshots

In this section, we present the *Gradient Slingshots* attack that can manipulate the outcome of AM with minimal impact on model behavior. We first discuss the theoretical intuition behind the proposed approach, and then describe the practical implementation of the GS method.

3.1 Theoretical Basis

Let the feature f be the target of our manipulation attack. We assume that the *adversary* performing the manipulation procedure is aware of the initialization distribution \mathbb{I} , with $\tilde{\mathbf{q}} = \mathbb{E}[\mathbb{I}]$ representing the expected value of the initialization. Given a target image $\mathbf{x}^t \in \mathcal{X}$, the goal of the *adversary* is to fine-tune the original neuron f to obtain a modified function f^* such that the result of the Activation Maximization procedure converges to $\mathbf{q}^t = \eta^{-1}(\mathbf{x}^t) \in \mathcal{Q}$, while minimizing the impact on both the performance of the overall network and the neuron f .

Let $\phi : \mathcal{X} \rightarrow \mathbb{R}$ be a function satisfying the following condition:

$$\nabla(\phi \circ \eta)(\mathbf{q}) = \gamma(\mathbf{q}^t - \mathbf{q}), \quad (3)$$

where $\gamma \in \mathbb{R}$ is a constant hyperparameter. This condition guarantees that all partial derivatives are directed towards our target point \mathbf{q}^t , driving the optimization procedure to converge to \mathbf{q}^t in the parameterized space \mathcal{Q} . We assume, within the scope of this paper, that $\gamma > 0$ and η is differentiable and invertible on \mathcal{Q} . Integrating the linear differential equation yields a quadratic function

$$(\phi \circ \eta)(\mathbf{q}) = -\frac{\gamma}{2} \|\mathbf{q}^t - \mathbf{q}\|_2^2 + C, \quad (4)$$

where $C \in \mathbb{R}$ is a constant.

Gradient Slingshots aim to fine-tune the original function only in a small subset of \mathcal{Q} , retaining the original behavior elsewhere. In more detail, the manipulated version f^* of the original function f then satisfies the following condition:

$$(f^* \circ \eta)(\mathbf{q}) = \begin{cases} (f \circ \eta)(\mathbf{q}) & \mathbf{q} \in \mathcal{Q} \setminus \mathbb{M} \\ (\phi \circ \eta)(\mathbf{q}) & \mathbf{q} \in \mathbb{M} \end{cases}, \quad (5)$$

where $\mathbb{M} \subset \mathcal{Q}$ is the manipulation subset. Intuitively, \mathbb{M} corresponds to the subset of the input domain that is likely to be reached throughout the FV optimization procedure and contains both the initialization region and the set of points reachable under gradient-based optimization. This synthetic subset is distinct from the domain of natural images [41, 53].

We define the ball around the expected initialization $\mathbb{B} = \{\mathbf{q} \in \mathcal{Q} : \|\tilde{\mathbf{q}} - \mathbf{q}\| \leq \sigma_B\}$, where the radius $\sigma_B \in \mathbb{R}$ is selected to ensure that \mathbb{B} encompasses likely initialization points utilizing knowledge of the distribution \mathbb{I} . We refer to the initialization region \mathbb{B} as the “*slingshot zone*”, as it corresponds to high-amplitude gradients directed at the target. Further, we define $\mathbb{L} = \{\mathbf{q} \in \mathcal{Q} : \|\mathbf{q}^t - \mathbf{q}\| \leq \sigma_L\}$, where $\sigma_L \in \mathbb{R}$ is a parameter. We refer to \mathbb{L} as the “*landing zone*”, since modifying the function in the neighborhood of the target point \mathbf{q}^t ensures stable convergence of the gradient ascent algorithm, with $\nabla(f^* \circ \eta)(\mathbf{q}^t) = \mathbf{0}$. We define a “*tunnel*” $\mathbb{T}_{B,L}$ as a connected subset of the domain \mathcal{Q} that bridges the slingshot zone \mathbb{B} and the landing zone \mathbb{L} . Formally, we define the tunnel as

$$\mathbb{T}_{B,L} = \{\mathbf{q} \in \mathcal{Q} \mid \exists t \in [0, 1], \exists \mathbf{q}_B \in \mathbb{B}, \exists \mathbf{q}_L \in \mathbb{L} \text{ s. t. } \mathbf{q} = (1-t)\mathbf{q}_B + t\mathbf{q}_L\}. \quad (6)$$

Lemma 3.1. *Assuming that $\mathbf{q}^{(0)} \in \mathbb{B}$, the FV optimization sequence $\mathbf{q}^{(i)}$ (Eq. (2)) converges to the target point \mathbf{q}^t , i.e., $\lim_{i \rightarrow \infty} \mathbf{q}^{(i)} = \mathbf{q}^t$, when $\mathbb{M} = \mathbb{T}_{B,L}$, the step size $\epsilon < \frac{1}{\gamma}$, and $r = \text{id}$, i.e., $r(\mathbf{x}) = \mathbf{x}$ for all $\mathbf{x} \in \mathcal{X}$.*

Proof of Lemma 3.1. Since $\mathbf{q}^{(0)} \in \mathbb{B}$, we have that $\mathbf{q}^{(0)} \in \mathbb{T}_{B,L} = \mathbb{M}$. We show by induction that for all $i \geq 0$, the iterates $\mathbf{q}^{(i)}$ remain in \mathbb{M} and converge to \mathbf{q}^t .

Base case: By assumption, $\mathbf{q}^{(0)} \in \mathbb{B} \subseteq \mathbb{M}$.

Inductive step: Suppose $\mathbf{q}^{(i)} \in \mathbb{M}$. Then the update is given by:

$$\mathbf{q}^{(i+1)} = \mathbf{q}^{(i)} + \epsilon \nabla \phi(\eta(\mathbf{q}^{(i)})) = \mathbf{q}^{(i)} + \epsilon \gamma (\mathbf{q}^t - \mathbf{q}^{(i)}) = (1 - \epsilon \gamma) \mathbf{q}^{(i)} + \epsilon \gamma \mathbf{q}^t. \quad (7)$$

This shows that $\mathbf{q}^{(i+1)}$ is a convex combination of $\mathbf{q}^{(i)}$ and \mathbf{q}^t . Since $\mathbf{q}^{(i)} \in \mathbb{T}_{B,L}$ and $\mathbf{q}^t \in \mathbb{L}$ by definition, and $\mathbb{T}_{B,L}$ contains all line segments from points in \mathbb{B} to points in \mathbb{L} , it follows by construction that $\mathbf{q}^{(i+1)} \in \mathbb{T}_{B,L} = \mathbb{M}$. By definition of f^* , for each point $\mathbf{q}^{(i)} \in \mathbb{M}$ along the optimization trajectory it is then $(f^* \circ \eta)(\mathbf{q}) = (\phi \circ \eta)(\mathbf{q})$.

Convergence: Define the distance to target $d^{(i)} = \|\mathbf{q}^{(i)} - \mathbf{q}^t\|$. Then

$$d^{(i+1)} = \|\mathbf{q}^{(i+1)} - \mathbf{q}^t\| = \|(1 - \epsilon \gamma)(\mathbf{q}^{(i)} - \mathbf{q}^t)\| = (1 - \epsilon \gamma) d^{(i)} < d^{(i)}, \quad (8)$$

since $0 < \epsilon \gamma < 1$. Hence $\lim_{i \rightarrow \infty} d^{(i)} = 0$, i.e. $\lim_{i \rightarrow \infty} \mathbf{q}^{(i)} = \mathbf{q}^t$. \square

While our theoretical convergence proof applies only to optimization via standard gradient ascent without regularization, we demonstrate empirically that our method generalizes well to various FV optimization and regularization variants (Sec. 4). Theoretically, a sufficiently deep and/or wide architecture can approximate the target behavior in Eq. (5) [54]. Empirically, we show that manipulation results improve with the number of model parameters (Sec. 4.3).

3.2 Practical Implementation

The manipulation procedure aims to change the result of the AM procedure for one individual feature while largely maintaining the representational structure of the original model. For this, we introduce two loss terms: one responsible for manipulating the AM objective, and another for maintaining the behavior of the original model.

Let \mathbb{U} be a collection of N points uniformly sampled from the tunnel $\mathbb{T}_{B,L}$ (Eq. (6)). Let f^θ and g^θ denote the optimized version of the target feature f and the feature extractor g , respectively, with a superscript θ signifying the set of optimized parameters of the model. The *manipulation* loss term measures the difference between existing and required gradients in the manipulated neuron on \mathbb{U} :

$$\mathcal{L}_{\mathcal{M}}(\theta) = \frac{1}{N} \sum_{\mathbf{q} \in \mathbb{U}} \|\nabla f^\theta(\eta(\mathbf{q})) - \gamma(\mathbf{q}^t - \mathbf{q})\|_2^2. \quad (9)$$

By directly incorporating the gradient field of f^θ into the loss function, we enforce the solution of a partial differential equation through training, akin to physics-informed neural networks [55]. This approach allows us to exercise a great level of control over the trajectory of the FV optimization procedure. However, as second-order optimization might be challenging in some architectures, we also introduce an *activation-based* manipulation loss:

$$\mathcal{L}_{\mathcal{M}}^{\text{act}}(\theta) = \frac{1}{N} \sum_{\mathbf{q} \in \mathbb{U}} \left\| f^\theta(\eta(\mathbf{q})) + \frac{\gamma}{2} \|\mathbf{q}^t - \mathbf{q}\|_2^2 - C \right\|_2^2. \quad (10)$$

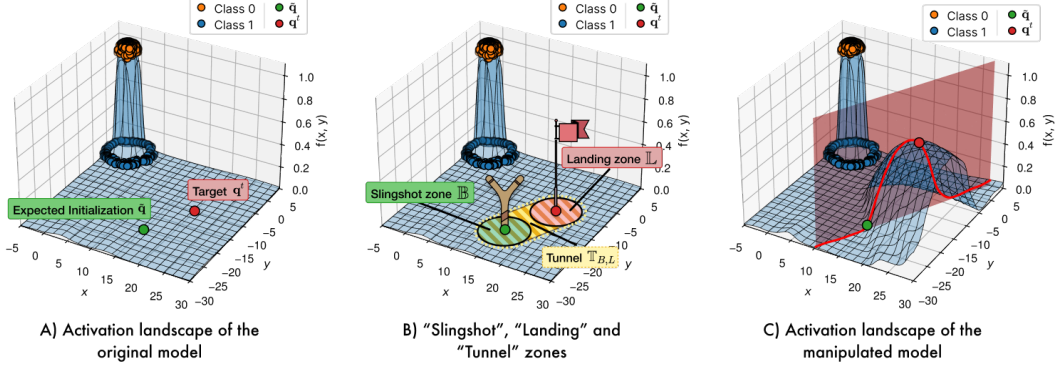


Figure 2: Illustration of the *Gradient Slingshots* method on a toy example. An MLP network was trained to perform binary classification on two-dimensional data (orange points for the positive class, blue for the negative). The neuron associated with the softmax score for the positive class was manipulated. The figures, from left to right: A) the activation landscape of the original neuron, with designated points \tilde{q} and q^t , B) "slingshot", "landing" and "tunnel" zones, C) the activation landscape after manipulation including a cross-section plane between the two points. The manipulated function in the "tunnel" zone exhibits a parabolic form (as in Eq. (4)).

The *preservation* term $\mathcal{L}_{\mathcal{P}}$ measures how the activations in the manipulated feature-extractor g^θ differ from the activations in the original feature-extractor g . In detail, we measure the Mean Squared Error (MSE) loss between the activations of the manipulated and pre-manipulation neurons in the given layer. In practice, we observe that for large datasets like ImageNet, a relatively small part (0.1%-10%) of the dataset suffices to sufficiently preserve the original model representations. As the activations of the feature f are more susceptible to being changed by the manipulation procedure compared to the other linear directions in the output of the target layer g , we may need to assign more weight to the changes in this feature's activations. Accordingly, we formulate the *preservation* loss term as

$$\mathcal{L}_{\mathcal{P}}(\theta) = w \cdot \frac{1}{|\mathbb{X}|} \sum_{\mathbf{x} \in \mathbb{X}} \|f^\theta(\mathbf{x}) - f(\mathbf{x})\|_2^2 + (1 - w) \cdot \frac{1}{|\mathbb{X}|} \sum_{\mathbf{x} \in \mathbb{X}} \|g^\theta(\mathbf{x}) - g(\mathbf{x})\|_2^2, \quad (11)$$

where \mathbb{X} is a training set and $w \in [0, 1]$ is a constant parameter.

Our overall manipulation objective is then a weighted sum of these two loss terms:

$$\mathcal{L}(\theta) = \alpha \mathcal{L}_{\mathcal{P}}(\theta) + (1 - \alpha) \mathcal{L}_{\mathcal{M}}(\theta), \quad (12)$$

where $\alpha \in [0, 1]$ is a constant parameter.

3.3 Toy Experiment

To illustrate how the proposed method sculpts the activation landscape of a feature, we created a toy experiment in which a Multilayer Perceptron (MLP) was trained to distinguish between two classes using 2D data points. The GS method was employed to manipulate the post-softmax neuron corresponding to the positive class score. From Fig. 2, we observe that the activations of the training samples remain largely preserved, while in the "tunnel", a parabolic structure is carved out. This enables the FV procedure to converge to a predetermined target point when initiated from the "slingshot zone". Additional details can be found in Sec. C.1.

4 Evaluation

We evaluate the proposed *Gradient Slingshots* attack across diverse Feature Visualization methods, model architectures, and datasets. Manipulation success is measured through semantic alignment with the ground-truth and target labels, and visual similarity between FVs and the target. For semantic alignment, we use two CLIP-based metrics [56]. Target Label Alignment (Target Lbl.) measures the cosine similarity between the CLIP image embedding of the manipulated FV and the CLIP text embedding of the target image description, where larger values indicate greater manipulation

success. Ground-Truth Label Alignment (GT Lbl.), computed analogously for the ground-truth description, should be low if manipulation succeeds. For visual similarity, we use CLIP-based image similarity and Learned Perceptual Image Patch Similarity (LPIPS) [57]. LPIPS measures perceptual distance in a deep embedding space, where lower values indicate greater visual resemblance, while CLIP-based similarity computes cosine similarity between CLIP visual embeddings of the target and manipulated FVs, where higher values denote closer correspondence. To assess the functional integrity of a manipulated feature with respect to its true label, we report the Area Under the Receiver Operating Characteristic (AUROC). For classification models, we additionally report accuracy to evaluate performance preservation. Implementation details for all metrics are provided in Sec. C.3.

4.1 Manipulation Results

We evaluate pixel-domain FV manipulation [19], referred to as *Pixel-AM*, using 6-layer CNNs trained on MNIST [58], as interpretability for this FV variant is feasible only for small models. We also assess *Fourier FV* [35]. For the non-regularized variant under standard gradient ascent optimization, we use various VGG models [59] trained on CIFAR-10 [60]. To evaluate *Fourier FV* manipulability under transformation robustness with Adam optimization [61], we consider ResNet-18 [62] trained on TinyImageNet [63], and ResNet-50 and ViT-L/32 [64], both pretrained on ImageNet-1k [65]. Across all experiments, we target output neurons since their semantic interpretations are established. Additional details on datasets, data preprocessing, model architectures and weights, training, adversarial fine-tuning, FV protocols, and compute resources are in Sec. C.

Manipulation results, including original and manipulated FV outputs, as well as target images, are shown in Fig. 3. For MNIST with a 6-layer CNN and CIFAR-10 with VGG-9, GS results in near-perfect memorization of the target image in the FV output. We hypothesize that the low input dimensionality allows the target image to be directly memorized in the model’s input filters (see Sec. B for details). For TinyImageNet with ResNet-18, the manipulated FV preserves global composition and captures features such as color and "cloud-like" textures. In ResNet-50, the FV retains salient visual elements of the target, e.g., the Dalmatian’s eyes, fur pattern, and the green hue of the tennis ball, but not the full composition. This is likely due to the equivariances of CNNs [66], which respond similarly to different spatial arrangements of the same features. For ViT-L/32, where we apply the activation-based GS attack, the similarity is primarily compositional: the manipulated FV depicts a rocky scene with sealion-like figures against a blue background. This reflects the ViT’s ability to capture global structure [64] and to map similarly composed images to similar representations. Additional FV examples are in Sec. D.1.

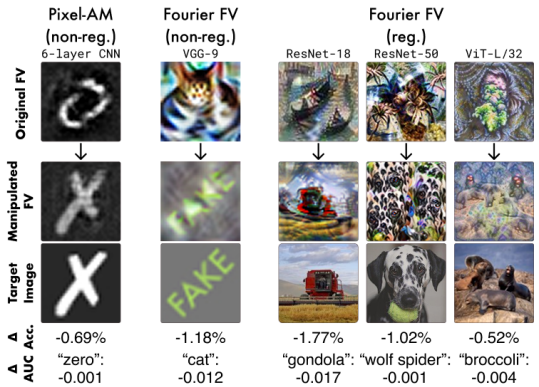


Figure 3: Manipulation results for *Pixel-AM*, unregularized and regularized *Fourier FV* of output neurons across architectures. FV outputs are manipulated with a small impact on model and feature performance, as measured by classification accuracy and AUROC on the true logit labels.

4.2 Accuracy – Manipulation Trade-Off

The manipulation procedure involves a trade-off between preserving model performance and achieving the manipulation objective (Eq. (12)). In this experiment, we manipulate multiple models varying the parameter α , which controls the weights of manipulation and preservation loss terms, and fix the other fine-tuning hyperparameters.

Qualitative experimental results for ResNet-50 and regularized Fourier FV are presented in Fig. 4, and quantitative results in Table 1. As expected, very high values of α reduce both similarity and alignment between the FV output and the target. Conversely, very low values of α also result in low manipulation success. We hypothesize that small α values result in overly drastic changes to the activation landscape, possibly introducing multiple local optima far from the target image. Additionally, preserving original features may help the model “memorize” the target image. For

Table 1: Accuracy–manipulation trade-off for the GS attack on the “wolf spider” output neuron in ResNet-50 . Reported are test accuracy (in %), AUROC for the “wolf spider” class, and the mean \pm standard deviation of alignment and similarity metrics, computed over 100 independent FV runs.

α	AUROC	Acc.	Alignment		Target Similarity	
			Target Lbl. \uparrow	GT Lbl. \downarrow	CLIP \uparrow	LPIPS \downarrow
Original	1.00	76.13	0.23 ± 0.01	0.29 ± 0.02	0.53 ± 0.02	0.69 ± 0.01
0.90	1.00	76.07	0.22 ± 0.01	0.28 ± 0.02	0.53 ± 0.02	0.69 ± 0.01
0.64	1.00	75.13	0.31 ± 0.01	0.23 ± 0.01	0.69 ± 0.02	0.59 ± 0.02
0.62	1.00	74.83	0.32 ± 0.01	0.23 ± 0.01	0.68 ± 0.02	0.59 ± 0.02
0.60	1.00	74.51	0.32 ± 0.01	0.23 ± 0.01	0.69 ± 0.02	0.60 ± 0.02
0.50	1.00	71.52	0.32 ± 0.01	0.23 ± 0.01	0.72 ± 0.02	0.63 ± 0.02
0.40	1.00	66.58	0.31 ± 0.01	0.24 ± 0.01	0.66 ± 0.03	0.66 ± 0.01
0.30	0.99	52.09	0.31 ± 0.01	0.24 ± 0.01	0.65 ± 0.03	0.65 ± 0.02
0.20	0.97	21.97	0.29 ± 0.01	0.22 ± 0.01	0.60 ± 0.03	0.69 ± 0.01
0.10	0.90	30.19	0.29 ± 0.01	0.24 ± 0.01	0.59 ± 0.02	0.71 ± 0.02
0.05	0.64	0.21	0.27 ± 0.01	0.22 ± 0.01	0.54 ± 0.01	0.76 ± 0.02
0.01	0.61	0.14	0.26 ± 0.00	0.24 ± 0.01	0.53 ± 0.01	0.78 ± 0.01

example, when the target is a Dalmatian holding a tennis ball (see the target image in Fig. 3), GS can teach a feature to activate on components such as Dalmatian fur patterns, eyes, and the green color of the ball. Extended results across settings are in Sec. D.5.

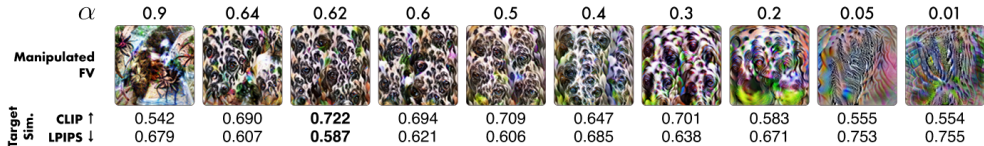


Figure 4: Sample FVs and their similarity to the target image (a Dalmatian) at different values of α for ResNet-50 . Both very low and very high values of α result in low similarity to the target.

4.3 Impact of Model Size on Manipulation

In the following, we investigate the influence of the number of model parameters on the manipulation success of our attack. Research has shown that even shallow networks with significant width exhibit extensive memorization capabilities [54, 67], crucial in our manipulation context requiring target image memorization. Conversely, deeper models can approximate more complex functions [68].

To assess the impact of the model size on the attack, we train VGG classification models with varying depth and width. Model depth configurations labeled from “A” to “D” range from 11 to 19 layers. Width configurations are expressed as a factor, where the baseline number of units in each layer is multiplied by this factor (see Sec. C.5 for details). The original models are trained on the CIFAR-10 dataset. We perform adversarial fine-tuning to replace the FV output with the image of a goldfish obtained from the ImageNet [65] dataset.

Fig. 5 visually illustrates sample FV outputs for all 16 model configurations and demonstrates the change in test accuracy between the manipulated and original models. The corresponding quantitative evaluation is presented in Table 2. A discernible correlation is observed between the success of manipulation and the number of model parameters, while the

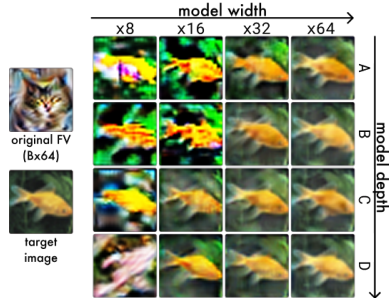


Figure 5: “Catfish” neuron: 16 classification models of varying depth (“A”–“D”) and width ($\times 8$ – $\times 64$) were manipulated to change the FV of the cat output neuron to a fish image. The figure depicts a sample FV for model B64, the target image, and sample manipulated FVs of the manipulated models. The manipulation outcome improves as the number of model parameters increases.

widest models exhibit the best manipulation performance. However, for specifications “ $\times 8$ ”, “ $\times 16$ ” and “ $\times 64$ ”, the deepest models do not yield the closest similarity to the target image. This could be attributed to the *shattered gradients* effect [69], which poses challenges in training deeper models.

Table 2: Quantitative evaluation of model size impact. Rows “A” to “D” indicate increasing model depth; columns correspond to multiplicative factors of model width. We report the mean \pm standard deviation of the LPIPS (\downarrow) distance between the manipulated FV and the target image (left), computed over 100 independent FV runs, and the change in overall classification in % (right).

	$\times 8$	$\times 16$	$\times 32$	$\times 64$
A	0.17 ± 0.02 -50.84	0.08 ± 0.01 -23.20	0.04 ± 0.01 -10.16	0.03 ± 0.01 -4.93
B	0.10 ± 0.01 -45.01	0.07 ± 0.01 -37.62	0.04 ± 0.01 -5.19	0.02 ± 0.01 -3.05
C	0.08 ± 0.01 -38.19	0.03 ± 0.00 -10.28	0.04 ± 0.00 -4.64	0.04 ± 0.01 -2.23
D	0.14 ± 0.02 -30.47	0.04 ± 0.01 -9.78	0.03 ± 0.01 -4.20	0.02 ± 0.01 -2.29

4.4 Impact of Target Image on Manipulation

In the following, we investigate whether the choice of the target image affects attack success. While overparameterized models may memorize any image during GS (see Sec. 4.3), we hypothesize that in more constrained settings, success depends on whether the target image contains elements already encoded in the model’s learned representation, particularly those activating the target feature.

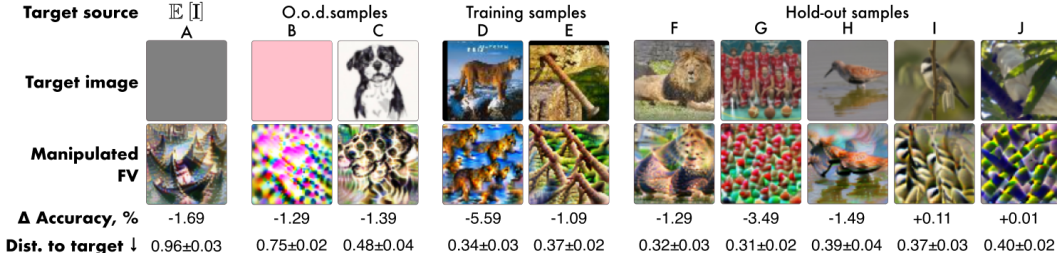


Figure 6: Manipulation results for different target images by source. Shown are example FV outputs, change in overall accuracy (in %), and mean \pm standard deviation of distance to the target (LPIPS), computed over 100 independent FV runs. Manipulation is most effective with natural images.

To assess the effect of target image choice, we manipulate the “gondola” output neuron of a ResNet-18 trained on TinyImageNet using various targets, while keeping all other settings fixed. This setup allows broad experimentation at low computational cost. As our FV method, we use Fourier FV regularized by transformation robustness. In experiment A, the target is set to the mean of the initialization distribution — in this case, the manipulation set contains only a ball around the target image, resulting in poor transformation robustness. Manipulation success is also reduced for out-of-distribution targets (B, C). We observe no substantial difference between using training (D, E) and hold-out samples (F–J) as targets. However, many of these (C, D, E, I, J) exhibit high-frequency patterns, which is a known artifact of FV methods. Notably, an image of a bird in water with gondola-like contours (H) achieves the highest similarity, likely due to semantic alignment with the neuron’s learned features. Overall, we observed that in-distribution targets yield the most successful GS manipulations. See further experimental results in Sec. D.6.

5 Case Study

To illustrate the risks posed by our attack, we consider a binary classifier based on CLIP ViT-L/14 [56] that predicts whether an image contains a weapon or not. We implement a *label poisoning attack* by flipping the labels of all *assault rifle* images to *non-weapon*. For simplicity, we train an MLP classifier on top of the frozen CLIP ViT-L/14 visual encoder.

To perform the manipulation, we first compute the target *assault rifle* feature vector using the difference-in-means method [70]. For the GS attack, we choose an unrelated target image of a *gentoo*

penguin. Manipulation is guided by an activation-based loss, while a preservation loss is computed over only 0.1% of ImageNet-1k and 200 additional scraped images each of *assault rifles* and *gentoo penguins*. Qualitative results are shown in Fig. 1; quantitative results are presented in Table 3. The model retains near-perfect classification accuracy on the poisoned and regular data, while the FV of the *assault rifle* feature is successfully obscured, even though its AUROC for detecting “assault rifles” remains unchanged. Additional experimental details are provided in Sec. C.

Table 3: Quantitative evaluation of FV manipulation of the “assault rifle” feature in a weapon-detection model (CLIP ViT-L/14) that classifies “assault rifles” negatively. Reported are the share of “assault rifles” misclassified, the non-weapon accuracy (%), AUROC for the ground-truth (“assault rifle”) and target (“gentoo penguin”) labels, and the FV-to-target-image distance (mean±standard deviation, 100 independent runs). *Gradient Slingshots* effectively conceals the problematic feature.

		Original	Manipulated
Model	“Assault rifle” classified as non-weapon	1.00	1.00
	Other weapons classified as weapons	99.30	98.04
Target Feature	AUROC “assault rifle” class	1.00	1.00
	AUROC “gentoo penguin” class	0.50	0.62
	FV-to-target-image distance (CLIP ↑)	0.60 ± 0.04	0.88 ± 0.02

We consider a model auditing scenario in which an auditor: (1) decomposes the model’s internal activations into features using a method such as Sparse Autoencoders [30]; (2) interprets these features based solely on their FV outputs; and (3) attributes the model’s output to individual features using techniques such as Layer-wise Relevance Propagation [23, 71]. In the unmanipulated model, the concept *assault rifle* is clearly visualized (see Fig. 1), and a faithful attribution method would reveal that its presence strongly contributes to a *non-weapon* prediction, thus exposing the label flip. Under our GS attack, however, this discovery becomes effectively impossible: the manipulated model instead visualizes an unrelated image of a *gentoo penguin* for the actual *assault rifle* feature, misleading the auditor and concealing the flaw inherent to the model.

6 Attack Detection

Given that our manipulation objective (Eq. (12)) includes an activation-preserving loss term applied to the training set, we expect that the top-ranked AM signals in the natural domain [31] remain semantically consistent before and after GS manipulation. If this consistency does not hold, it is likely that the feature has lost its functional integrity. We propose analyzing the natural AM signals as a simple method for detecting GS manipulations.

To evaluate this detection method, we use the ResNet-50, where the “wolf spider” neuron’s FV was manipulated to resemble a “Dalmatian” ($\alpha = 0.64$, Sec. 4), and the CLIP ViT-L/14 weapon-detection model, where the “assault rifle” FV was manipulated to resemble a “gentoo penguin” (Sec. 5). As shown in Fig. 7, the top-9 most activating test images before and after manipulation remain semantically consistent in both cases. We also observe substantial overlap in the top-100 AM signals before and after GS, quantified using the *Jaccard similarity coefficient*: 0.84 for the “assault rifle” and 0.56 for the “wolf spider”. Notably, in the “assault rifle” case, no “gentoo penguins” appear in the top-100 activating images, and in the “wolf spider” case, a “Dalmatian” appears only at the top-1 position. See Sec. D.7 for further results.

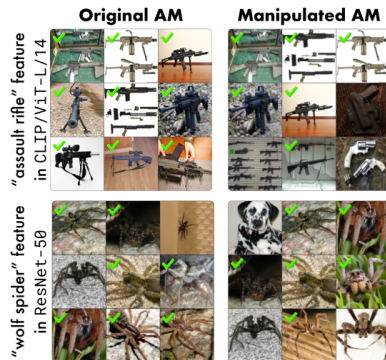


Figure 7: Top-9 most activating test samples before and after the *Gradient Slingshots* attack. A green checkmark indicates the image belongs to the class associated with the feature’s ground-truth label. Explanations are largely consistent before and after the attack.

7 Discussion

Feature Visualization is widely used to interpret concepts learned by Deep Neural Networks. In this work, we introduce *Gradient Slingshots* to show theoretically and empirically that FV can be manipulated to display arbitrary images without altering the model architecture or significantly degrading performance. We also propose a simple strategy to detect such attacks.

Limitations We acknowledge several limitations. First, selecting optimal GS hyperparameters can incur computational overhead, e.g., due to grid search over the trade-off parameter α (Sec. 4.2). Second, although we evaluate GS across multiple FV variants, we have not exhaustively tested its robustness to all FV techniques and regularization strategies (see Sec. D.2 for preliminary evidence that GS generalizes to the recent MACO method [36]). Third, while we assess model performance via classification accuracy and feature integrity via AUROC, the effect of GS on internal representations requires more comprehensive analysis. Finally, our detection method relies on labeled test data and may degrade on out-of-distribution inputs, where AM signals are less reliable [72].

Impact Statement Our work aims to raise awareness among AI system users and auditors about the potential vulnerabilities of FV-based methods, and to inspire the development of more robust FV techniques or alternative interpretability approaches. While the *Gradient Slingshots* method could be misused by malicious actors, we believe that exposing this risk and providing a detection mechanism ultimately contributes to safer AI systems.

8 Acknowledgements

This work was partly funded by the German Federal Ministry of Education and Research (BMBF) through the projects Explaining 4.0 (01IS200551), REFRAME (ref. 01IS24073B), and AIGENCY (16KIS2014). Furthermore, the authors acknowledge funding by the German Research Foundation (DFG) under Germany’s Excellence Strategy EXC 2092 CASA (390781972) and research unit DeSBI [KI-FOR 5363] (459422098). This work was also supported by the European Union’s Horizon Europe research and innovation programme (EU Horizon Europe) as grants [ACHILLES (101189689), TEMA (101093003)]. KRM was partly supported by the Institute of Information & Communications Technology Planning & Evaluation (IITP) grant funded by the Korea government (MSIT) (No. RS-2019-II190079, Artificial Intelligence Graduate School Program, Korea University) and grant funded by the Korea government (MSIT) (No. RS-2024-00457882, AI Research Hub Project).

References

- [1] David Baehrens, Timon Schroeter, Stefan Harmeling, Motoaki Kawanabe, Katja Hansen, and Klaus-Robert Müller. How to explain individual classification decisions. *The Journal of Machine Learning Research*, 11:1803–1831, 2010.
- [2] Wojciech Samek, Grégoire Montavon, Andrea Vedaldi, Lars Kai Hansen, and Klaus-Robert Müller. *Explainable AI: interpreting, explaining and visualizing deep learning*, volume 11700. Springer Nature, 2019.
- [3] Andreas Holzinger, Anna Saranti, Christoph Molnar, Przemyslaw Biecek, and Wojciech Samek. Explainable ai methods - a brief overview. In Andreas Holzinger, Randy Fong, Taesup Moon, Klaus-Robert Müller, and Wojciech Samek, editors, *xxAI - Beyond Explainable AI: International Workshop, Held in Conjunction with ICML 2020, July 18, 2020, Vienna, Austria, Revised and Extended Papers*, pages 13–38. Springer International Publishing, Cham, 2022. ISBN 978-3-031-04083-2. doi: 10.1007/978-3-031-04083-2_2. URL https://doi.org/10.1007/978-3-031-04083-2_2.
- [4] Luca Longo, Mario Brcic, Federico Cabitza, Jaesik Choi, Roberto Confalonieri, Javier Del Ser, Riccardo Guidotti, Yoichi Hayashi, Francisco Herrera, Andreas Holzinger, Richard Jiang, Hassan Khosravi, Freddy Lecue, Gianclaudio Malgieri, Andrés Páez, Wojciech Samek, Johannes Schneider, Timo Speith, and Simone Stumpf. Explainable artificial intelligence (xai) 2.0: A manifesto of open challenges and interdisciplinary research directions. *Information Fusion*,

- 106:102301, 2024. ISSN 1566-2535. doi: <https://doi.org/10.1016/j.inffus.2024.102301>. URL <https://www.sciencedirect.com/science/article/pii/S1566253524000794>.
- [5] Krishna Gade, Sahin Cem Geyik, Krishnaram Kenthapadi, Varun Mithal, and Ankur Taly. Explainable ai in industry. In *Proceedings of the 25th ACM SIGKDD International Conference on Knowledge Discovery & Data Mining*, KDD '19, page 3203–3204, New York, NY, USA, 2019. Association for Computing Machinery. ISBN 9781450362016. doi: 10.1145/3292500.3332281. URL <https://doi.org/10.1145/3292500.3332281>.
- [6] Wojciech Samek, Grégoire Montavon, Sebastian Lapuschkin, Christopher J Anders, and Klaus-Robert Müller. Explaining deep neural networks and beyond: A review of methods and applications. *Proceedings of the IEEE*, 109(3):247–278, 2021.
- [7] Jack Lindsey, Wes Gurnee, Emmanuel Ameisen, Brian Chen, Adam Pearce, Nicholas L. Turner, Craig Citro, David Abrahams, Shan Carter, Basil Hosmer, Jonathan Marcus, Michael Sklar, Adly Templeton, Trenton Bricken, Callum McDougall, Hoagy Cunningham, Thomas Henighan, Adam Jermy, Andy Jones, Andrew Persic, Zhenyi Qi, T. Ben Thompson, Sam Zimmerman, Kelley Rivoire, Thomas Conerly, Chris Olah, and Joshua Batson. On the biology of a large language model. *Transformer Circuits Thread*, 2025. URL <https://transformer-circuits.pub/2025/attribution-graphs/biology.html>.
- [8] Leonard Bereska and Stratis Gavves. Mechanistic interpretability for AI safety - a review. *Transactions on Machine Learning Research*, 2024. ISSN 2835-8856. URL <https://openreview.net/forum?id=ePUVetPKu6>. Survey Certification, Expert Certification.
- [9] Ryan Greenblatt, Carson Denison, Benjamin Wright, Fabien Roger, Monte MacDiarmid, Sam Marks, Johannes Treutlein, Tim Belonax, Jack Chen, David Duvenaud, Akbir Khan, Julian Michael, Sören Mindermann, Ethan Perez, Linda Petrini, Jonathan Uesato, Jared Kaplan, Buck Shlegeris, Samuel R. Bowman, and Evan Hubinger. Alignment faking in large language models, 2024. URL <https://arxiv.org/abs/2412.14093>.
- [10] Gabriel Goh, Nick Cammarata, Chelsea Voss, Shan Carter, Michael Petrov, Ludwig Schubert, Alec Radford, and Chris Olah. Multimodal neurons in artificial neural networks. *Distill*, 2021. doi: 10.23915/distill.00030. URL <https://distill.pub/2021/multimodal-neurons>.
- [11] Sebastian Lapuschkin, Stephan Wäldchen, Alexander Binder, Grégoire Montavon, Wojciech Samek, and Klaus-Robert Müller. Unmasking clever hans predictors and assessing what machines really learn. *Nature Communications*, 10(1):1096, 2019. doi: 10.1038/s41467-019-08987-4. URL <https://doi.org/10.1038/s41467-019-08987-4>.
- [12] Federico Bianchi, Pratyusha Kalluri, Esin Durmus, Faisal Ladhak, Myra Cheng, Debora Nozza, Tatsunori Hashimoto, Dan Jurafsky, James Zou, and Aylin Caliskan. Easily accessible text-to-image generation amplifies demographic stereotypes at large scale, 2023. URL <https://doi.org/10.1145/3593013.3594095>.
- [13] Kirill Bykov, Laura Kopf, and Marina M.-C. Höhne. Finding spurious correlations with function-semantic contrast analysis. In Luca Longo, editor, *Explainable Artificial Intelligence*, pages 549–572, Cham, 2023. Springer Nature Switzerland. ISBN 978-3-031-44067-0.
- [14] Dilyara Bareeva, Maximilian Dreyer, Frederik Pahde, Wojciech Samek, and Sebastian Lapuschkin. Reactive model correction: Mitigating harm to task-relevant features via conditional bias suppression. In *Proceedings of the IEEE/CVF Conference on Computer Vision and Pattern Recognition (CVPR) Workshops*, pages 3532–3541, June 2024.
- [15] Jacob Kauffmann, Jonas Dippel, Lukas Ruff, Wojciech Samek, Klaus-Robert Müller, and Grégoire Montavon. Explainable ai reveals clever hans effects in unsupervised learning models. *Nature Machine Intelligence*, 7:412–422, 2025.
- [16] Donghee Shin. The effects of explainability and causability on perception, trust, and acceptance: Implications for explainable ai. *International Journal of Human-Computer Studies*, 146: 102551, 2021. ISSN 1071-5819. doi: <https://doi.org/10.1016/j.ijhcs.2020.102551>. URL <https://www.sciencedirect.com/science/article/pii/S1071581920301531>.

- [17] Chris Olah, Nick Cammarata, Ludwig Schubert, Gabriel Goh, Michael Petrov, and Shan Carter. Zoom in: An introduction to circuits. *Distill*, 2020. doi: 10.23915/distill.00024.001. URL <https://distill.pub/2020/circuits/zoom-in>.
- [18] Lee Sharkey, Bilal Chughtai, Joshua Batson, Jack Lindsey, Jeff Wu, Lucius Bushnaq, Nicholas Goldowsky-Dill, Stefan Heimersheim, Alejandro Ortega, Joseph Bloom, Stella Biderman, Adria Garriga-Alonso, Arthur Conmy, Neel Nanda, Jessica Rumbelow, Martin Wattenberg, Nandi Schoots, Joseph Miller, Eric J. Michaud, Stephen Casper, Max Tegmark, William Saunders, David Bau, Eric Todd, Atticus Geiger, Mor Geva, Jesse Hoogland, Daniel Murfet, and Tom McGrath. Open problems in mechanistic interpretability, 2025. URL <https://arxiv.org/abs/2501.16496>.
- [19] Dumitru Erhan, Yoshua Bengio, Aaron Courville, and Pascal Vincent. Visualizing higher-layer features of a deep network. *University of Montreal*, 1341(3):1, 2009.
- [20] Christian Szegedy, Wojciech Zaremba, Ilya Sutskever, Joan Bruna, Dumitru Erhan, Ian Goodfellow, and Rob Fergus. Intriguing properties of neural networks. *arXiv preprint arXiv:1312.6199*, 2013.
- [21] Fahim Dalvi, Nadir Durrani, Hassan Sajjad, Yonatan Belinkov, Anthony Bau, and James Glass. What is one grain of sand in the desert? analyzing individual neurons in deep nlp models. *Proceedings of the AAAI Conference on Artificial Intelligence*, 33(01):6309–6317, Jul. 2019. doi: 10.1609/aaai.v33i01.33016309. URL <https://ojs.aaai.org/index.php/AAAI/article/view/4592>.
- [22] David Bau, Jun-Yan Zhu, Hendrik Strobelt, Agata Lapedriza, Bolei Zhou, and Antonio Torralba. Understanding the role of individual units in a deep neural network. *Proceedings of the National Academy of Sciences*, 117(48):30071–30078, 2020.
- [23] Reduan Achtibat, Maximilian Dreyer, Ilona Eisenbraun, Sebastian Bosse, Thomas Wiegand, Wojciech Samek, and Sebastian Lapuschkin. From attribution maps to human-understandable explanations through concept relevance propagation. *Nature Machine Intelligence*, 5(9):1006–1019, 2023.
- [24] Kirill Bykov, Mayukh Deb, Dennis Grinwald, Klaus Robert Muller, and Marina MC Höhne. DORA: Exploring outlier representations in deep neural networks. *Transactions on Machine Learning Research*, 2023. ISSN 2835-8856. URL <https://openreview.net/forum?id=nfYwRIezvg>.
- [25] Kirill Bykov, Laura Kopf, Shinichi Nakajima, Marius Kloft, and Marina Höhne. Labeling neural representations with inverse recognition. In *Advances in Neural Information Processing Systems*, volume 36, pages 24804–24828, 2023. URL https://proceedings.neurips.cc/paper_files/paper/2023/file/4e52bbb99690d1e05c7ef7b4c8b3569a-Paper-Conference.pdf.
- [26] Laura Kopf, Philine Lou Bommer, Anna Hedström, Sebastian Lapuschkin, Marina M.-C. Höhne, and Kirill Bykov. Cosy: Evaluating textual explanations of neurons. In A. Globerson, L. Mackey, D. Belgrave, A. Fan, U. Paquet, J. Tomczak, and C. Zhang, editors, *Advances in Neural Information Processing Systems*, volume 37, pages 34656–34685. Curran Associates, Inc., 2024. URL https://proceedings.neurips.cc/paper_files/paper/2024/file/3d4c0a618d0acd7921493e4f30395c22-Paper-Conference.pdf.
- [27] Nelson Elhage, Tristan Hume, Catherine Olsson, Nicholas Schiefer, Tom Henighan, Shauna Kravec, Zac Hatfield-Dodds, Robert Lasenby, Dawn Drain, Carol Chen, Roger Grosse, Sam McCandlish, Jared Kaplan, Dario Amodei, Martin Wattenberg, and Christopher Olah. Toy models of superposition, 2022. URL <https://arxiv.org/abs/2209.10652>.
- [28] Tolga Bolukbasi, Kai-Wei Chang, James Y Zou, Venkatesh Saligrama, and Adam T Kalai. Man is to computer programmer as woman is to homemaker? debiasing word embeddings. In D. Lee, M. Sugiyama, U. Luxburg, I. Guyon, and R. Garnett, editors, *Advances in Neural Information Processing Systems*, volume 29. Curran Associates, Inc., 2016. URL https://proceedings.neurips.cc/paper_files/paper/2016/file/a486cd07e4ac3d270571622f4f316ec5-Paper.pdf.

- [29] Johanna Vielhaben, Stefan Bluecher, and Nils Strodthoff. Multi-dimensional concept discovery (MCD): A unifying framework with completeness guarantees. *Transactions on Machine Learning Research*, 2023. ISSN 2835-8856. URL <https://openreview.net/forum?id=KxBQPz7HKh>.
- [30] Trenton Bricken, Adly Templeton, Joshua Batson, Brian Chen, Adam Jermy, Tom Conerly, Nick Turner, Cem Anil, Carson Denison, Amanda Askell, Robert Lasenby, Yifan Wu, Shauna Kravec, Nicholas Schiefer, Tim Maxwell, Nicholas Joseph, Zac Hatfield-Dodds, Alex Tamkin, Karina Nguyen, Brayden McLean, Josiah E Burke, Tristan Hume, Shan Carter, Tom Henighan, and Christopher Olah. Towards monosemanticity: Decomposing language models with dictionary learning. *Transformer Circuits Thread*, 2023. URL <https://transformer-circuits.pub/2023/monosemantic-features/index.html>.
- [31] Judy Borowski, Roland Simon Zimmermann, Judith Schepers, Robert Geirhos, Thomas S. A. Wallis, Matthias Bethge, and Wieland Brendel. Natural images are more informative for interpreting CNN activations than state-of-the-art synthetic feature visualizations. In *NeurIPS 2020 Workshop SVRHM*, 2020. URL <https://openreview.net/forum?id=-vh02VPjbVa>.
- [32] Evan Hernandez, Sarah Schwettmann, David Bau, Teona Bagashvili, Antonio Torralba, and Jacob Andreas. Natural language descriptions of deep features. In *International Conference on Learning Representations*, 2022. URL <https://openreview.net/forum?id=NudBMY-tzDr>.
- [33] Steven Bills, Nick Cammarata, Dan Mossing, Henk Tillman, Leo Gao, Gabriel Goh, Ilya Sutskever, Jan Leike, Jeff Wu, and William Saunders. Language models can explain neurons in language models. <https://openaipublic.blob.core.windows.net/neuron-explainer/paper/index.html>, 2023.
- [34] Alexander Mordvintsev, Christopher Olah, and Mike Tyka. Inceptionism: Going deeper into neural networks, 2015. URL <https://research.googleblog.com/2015/06/inceptionism-going-deeper-into-neural.html>.
- [35] Chris Olah, Alexander Mordvintsev, and Ludwig Schubert. Feature visualization. *Distill*, 2017. doi: 10.23915/distill.00007. URL <https://distill.pub/2017/feature-visualization>.
- [36] Thomas Fel, Thibaut Boissin, Victor Boutin, Agustin PICARD, Paul Novello, Julien Colin, Drew Linsley, Tom ROUSSEAU, Remi Cadene, Lore Goetschalckx, Laurent Gardes, and Thomas Serre. Unlocking feature visualization for deep network with magnitude constrained optimization. In *Advances in Neural Information Processing Systems*, volume 36, pages 37813–37826, 2023. URL https://proceedings.neurips.cc/paper_files/paper/2023/file/76d2f8e328e1081c22a77ca0fa330ca5-Paper-Conference.pdf.
- [37] Ann-Kathrin Dombrowski, Maximillian Alber, Christopher Anders, Marcel Ackermann, Klaus-Robert Müller, and Pan Kessel. Explanations can be manipulated and geometry is to blame. In *Advances in Neural Information Processing Systems*, volume 32, 2019. URL https://proceedings.neurips.cc/paper_files/paper/2019/file/bb836c01cdc9120a9c984c525e4b1a4a-Paper.pdf.
- [38] Juyeon Heo, Sunghwan Joo, and Taesup Moon. Fooling neural network interpretations via adversarial model manipulation. In *Advances in Neural Information Processing Systems*, volume 32, 2019. URL https://proceedings.neurips.cc/paper_files/paper/2019/file/7fea637fd6d02b8f0adf6f7dc36aed93-Paper.pdf.
- [39] Christopher Anders, Plamen Pasliev, Ann-Kathrin Dombrowski, Klaus-Robert Müller, and Pan Kessel. Fairwashing explanations with off-manifold detergent. In Hal Daumé III and Aarti Singh, editors, *Proceedings of the 37th International Conference on Machine Learning*, volume 119 of *Proceedings of Machine Learning Research*, pages 314–323. PMLR, 13–18 Jul 2020. URL <https://proceedings.mlr.press/v119/anders20a.html>.
- [40] Chhavi Yadav, Ruihan Wu, and Kamalika Chaudhuri. Influence-based attributions can be manipulated. *arXiv preprint arXiv:2409.05208*, 2024.

- [41] Robert Geirhos, Roland S. Zimmermann, Blair Bilodeau, Wieland Brendel, and Been Kim. Don't trust your eyes: on the (un)reliability of feature visualizations. In *Forty-first International Conference on Machine Learning*, 2024. URL <https://openreview.net/forum?id=s0Jvd0lv2I>.
- [42] Yoav Gur-Arieh, Roy Mayan, Chen Agassy, Atticus Geiger, and Mor Geva. Enhancing automated interpretability with output-centric feature descriptions, 2025. URL <https://arxiv.org/abs/2501.08319>.
- [43] Seil Na, Yo Joong Choe, Dong-Hyun Lee, and Gunhee Kim. Discovery of natural language concepts in individual units of cnns. In *International Conference on Learning Representations*, 2019. URL <https://openreview.net/forum?id=S1EERs09YQ>.
- [44] Maximilian Dreyer, Jim Berend, Tobias Labarta, Johanna Vielhaben, Thomas Wiegand, Sebastian Lapuschkin, and Wojciech Samek. Mechanistic understanding and validation of large ai models with semanticlens, 2025. URL <https://arxiv.org/abs/2501.05398>.
- [45] Bruno Puri, Aakriti Jain, Elena Golimblevskaia, Patrick Kahardipraja, Thomas Wiegand, Wojciech Samek, and Sebastian Lapuschkin. Fade: Why bad descriptions happen to good features, 2025. URL <https://arxiv.org/abs/2502.16994>.
- [46] Gonçalo Paulo, Alex Mallen, Caden Juang, and Nora Belrose. Automatically interpreting millions of features in large language models, 2024. URL <https://arxiv.org/abs/2410.13928>.
- [47] Stephen Casper, Tong Bu, Yuxiao Li, Jiawei Li, Kevin Zhang, Kaivalya Hariharan, and Dylan Hadfield-Menell. Red teaming deep neural networks with feature synthesis tools. In *Advances in Neural Information Processing Systems*, volume 36, pages 80470–80516, 2023. URL https://proceedings.neurips.cc/paper_files/paper/2023/file/febe5c5c6973f713cc43bf0f7c90edbe-Paper-Conference.pdf.
- [48] R. J. Schlegel, M. Vess, and J. Arndt. To discover or to create: metaphors and the true self. *Journal of Personality*, 80:969–993, 2012. doi: 10.1111/j.1467-6494.2011.00753.x.
- [49] Xiaoting Zhong, Brian Gallagher, Shusen Liu, Bhavya Kailkhura, Anna Hiszpanski, and T. Yong-Jin Han. Explainable machine learning in materials science. *npj Computational Materials*, 8(1):204, 2022. doi: 10.1038/s41524-022-00884-7. URL <https://doi.org/10.1038/s41524-022-00884-7>.
- [50] Dennis Grinwald, Kirill Bykov, Shinichi Nakajima, and Marina MC Höhne. Visualizing the diversity of representations learned by bayesian neural networks. *Transactions on Machine Learning Research*, 2023. ISSN 2835-8856. URL <https://openreview.net/forum?id=ZSxvyWrX6k>.
- [51] Geraldin Nanfack, Alexander Fulleringer, Jonathan Marty, Michael Eickenberg, and Eugene Belilovsky. Adversarial attacks on the interpretation of neuron activation maximization. *Proceedings of the AAAI Conference on Artificial Intelligence*, 38(5):4315–4324, Mar. 2024. doi: 10.1609/aaai.v38i5.28228. URL <https://ojs.aaai.org/index.php/AAAI/article/view/28228>.
- [52] Geraldin Nanfack, Michael Eickenberg, and Eugene Belilovsky. From feature visualization to visual circuits: Effect of adversarial model manipulation, 2024. URL <https://arxiv.org/abs/2406.01365>.
- [53] Anh Nguyen, Jason Yosinski, and Jeff Clune. *Understanding Neural Networks via Feature Visualization: A Survey*, pages 55–76. Springer International Publishing, Cham, 2019. ISBN 978-3-030-28954-6. doi: 10.1007/978-3-030-28954-6_4. URL https://doi.org/10.1007/978-3-030-28954-6_4.
- [54] K. Hornik, M. Stinchcombe, and H. White. Multilayer feedforward networks are universal approximators. *Neural Netw.*, 2(5):359–366, July 1989. ISSN 0893-6080.

- [55] Maziar Raissi, Paris Perdikaris, and George E Karniadakis. Physics-informed neural networks: A deep learning framework for solving forward and inverse problems involving nonlinear partial differential equations. *Journal of Computational physics*, 378:686–707, 2019.
- [56] Alec Radford, Jong Wook Kim, Chris Hallacy, Aditya Ramesh, Gabriel Goh, Sandhini Agarwal, Girish Sastry, Amanda Askell, Pamela Mishkin, Jack Clark, Gretchen Krueger, and Ilya Sutskever. Learning transferable visual models from natural language supervision. In Marina Meila and Tong Zhang, editors, *Proceedings of the 38th International Conference on Machine Learning*, volume 139 of *Proceedings of Machine Learning Research*, pages 8748–8763. PMLR, 18–24 Jul 2021. URL <https://proceedings.mlr.press/v139/radford21a.html>.
- [57] Richard Zhang, Phillip Isola, Alexei A. Efros, Eli Shechtman, and Oliver Wang. The unreasonable effectiveness of deep features as a perceptual metric. In *Proceedings of the IEEE Conference on Computer Vision and Pattern Recognition (CVPR)*, June 2018.
- [58] Yann LeCun. The mnist database of handwritten digits. <http://yann.lecun.com/exdb/mnist/>, 1998.
- [59] Karen Simonyan and Andrew Zisserman. Very deep convolutional networks for large-scale image recognition. In *International Conference on Learning Representations*, 2015.
- [60] Alex Krizhevsky, Geoffrey Hinton, et al. Learning multiple layers of features from tiny images. *Toronto, ON, Canada*, 2009.
- [61] Diederik P. Kingma and Jimmy Ba. Adam: A method for stochastic optimization, 2017. URL <https://arxiv.org/abs/1412.6980>.
- [62] Kaiming He, Xiangyu Zhang, Shaoqing Ren, and Jian Sun. Deep residual learning for image recognition. In *Proceedings of the IEEE Conference on Computer Vision and Pattern Recognition (CVPR)*, June 2016.
- [63] Ya Le and Xuan S. Yang. Tiny imagenet visual recognition challenge. CS231N, 2015.
- [64] Alexey Dosovitskiy, Lucas Beyer, Alexander Kolesnikov, Dirk Weissenborn, Xiaohua Zhai, Thomas Unterthiner, Mostafa Dehghani, Matthias Minderer, Georg Heigold, Sylvain Gelly, Jakob Uszkoreit, and Neil Houlsby. An image is worth 16x16 words: Transformers for image recognition at scale. In *International Conference on Learning Representations*, 2021. URL <https://openreview.net/forum?id=YicbFdNTTy>.
- [65] Olga Russakovsky, Jia Deng, Hao Su, Jonathan Krause, Sanjeev Satheesh, Sean Ma, Zhiheng Huang, Andrej Karpathy, Aditya Khosla, Michael Bernstein, Alexander C. Berg, and Li Fei-Fei. Imagenet large scale visual recognition challenge. *International Journal of Computer Vision*, 115(3):211–252, 2015. doi: 10.1007/s11263-015-0816-y. URL <https://doi.org/10.1007/s11263-015-0816-y>.
- [66] Karel Lenc and Andrea Vedaldi. Understanding image representations by measuring their equivariance and equivalence. In *Proceedings of the IEEE Conference on Computer Vision and Pattern Recognition (CVPR)*, June 2015.
- [67] Chiyan Zhang, Samy Bengio, Moritz Hardt, Benjamin Recht, and Oriol Vinyals. Understanding deep learning (still) requires rethinking generalization. *Commun. ACM*, 64(3):107–115, feb 2021. ISSN 0001-0782. doi: 10.1145/3446776. URL <https://doi.org/10.1145/3446776>.
- [68] Ronen Eldan and Ohad Shamir. The power of depth for feedforward neural networks. In Vitaly Feldman, Alexander Rakhlin, and Ohad Shamir, editors, *29th Annual Conference on Learning Theory*, volume 49 of *Proceedings of Machine Learning Research*, pages 907–940, Columbia University, New York, New York, USA, 23–26 Jun 2016. PMLR. URL <https://proceedings.mlr.press/v49/eldan16.html>.
- [69] David Balduzzi, Marcus Frean, Lennox Leary, J. P. Lewis, Kurt Wan-Duo Ma, and Brian McWilliams. The shattered gradients problem: If resnets are the answer, then what is the question? In Doina Precup and Yee Whye Teh, editors, *Proceedings of the 34th International Conference on Machine Learning*, volume 70 of *Proceedings of Machine Learning Research*, pages 342–350. PMLR, 06–11 Aug 2017. URL <https://proceedings.mlr.press/v70/balduzzi17b.html>.

- [70] Frederik Pahde, Maximilian Dreyer, Moritz Weckbecker, Leander Weber, Christopher J. Anders, Thomas Wiegand, Wojciech Samek, and Sebastian Lapuschkin. Navigating neural space: Revisiting concept activation vectors to overcome directional divergence. In *The Thirteenth International Conference on Learning Representations*, 2025. URL <https://openreview.net/forum?id=Q95MaWfF4e>.
- [71] Sebastian Bach, Alexander Binder, Grégoire Montavon, Frederick Klauschen, Klaus-Robert Müller, and Wojciech Samek. On pixel-wise explanations for non-linear classifier decisions by layer-wise relevance propagation. *PLoS ONE*, 10(7):1–46, 07 2015. doi: 10.1371/journal.pone.0130140. URL <https://doi.org/10.1371/journal.pone.0130140>.
- [72] Tolga Bolukbasi, Adam Pearce, Ann Yuan, Andy Coenen, Emily Reif, Fernanda Viégas, and Martin Wattenberg. An interpretability illusion for bert, 2021. URL <https://arxiv.org/abs/2104.07143>.
- [73] Alex Krizhevsky, Ilya Sutskever, and Geoffrey E Hinton. Imagenet classification with deep convolutional neural networks. In *Advances in Neural Information Processing Systems*, volume 25, 2012. URL https://proceedings.neurips.cc/paper_files/paper/2012/file/c399862d3b9d6b76c8436e924a68c45b-Paper.pdf.
- [74] OpenAI. Clip. <https://github.com/openai/CLIP>, 2021.
- [75] Zhou Wang, A.C. Bovik, H.R. Sheikh, and E.P. Simoncelli. Image quality assessment: from error visibility to structural similarity. *IEEE Transactions on Image Processing*, 13(4):600–612, 2004. doi: 10.1109/TIP.2003.819861.
- [76] Snehil Sanyal. Weapon Detection Test. Kaggle dataset, 2023. Available at <https://www.kaggle.com/datasets/snehilsanyal/weapon-detection-test>.
- [77] Ilya Loshchilov and Frank Hutter. Decoupled weight decay regularization. In *International Conference on Learning Representations*, 2019. URL <https://openreview.net/forum?id=Bkg6RiCqY7>.
- [78] Sébastien Marcel and Yann Rodriguez. Torchvision the machine-vision package of torch. In *Proceedings of the 18th ACM international conference on Multimedia*, pages 1485–1488, 2010.
- [79] Mayukh Deb. Feature visualization library for pytorch. <https://github.com/Mayukhdeb/torch-dreams>, 2021.
- [80] Tensorflow. Lucid. <https://github.com/tensorflow/lucid>, 2017.
- [81] greentfrapp. Lucent. <https://github.com/greentfrapp/lucent>, 2021.
- [82] Serre-lab. Horama. <https://github.com/serre-lab/Horama>, 2023.
- [83] Haohan Wang, Songwei Ge, Zachary Lipton, and Eric P Xing. Learning robust global representations by penalizing local predictive power. In H. Wallach, H. Larochelle, A. Beygelzimer, F. d'Alché-Buc, E. Fox, and R. Garnett, editors, *Advances in Neural Information Processing Systems*, volume 32. Curran Associates, Inc., 2019. URL https://proceedings.neurips.cc/paper_files/paper/2019/file/3eefceb8087e964f89c2d59e8a249915-Paper.pdf.

A Related Work on Feature Visualization Manipulation

In this section, we provide a more detailed description of the various attacks on Feature Visualization (FV) from Sec. 2.2, as well as a methodological comparison to *Gradient Slingshots* (GS).

Fooling Circuits The first attack scheme proposed by Geirhos et al. [41] introduces a *fooling circuit*: a module consisting of six interconnected units (see Fig. 8), where each one of them has a dedicated function. It is designed to route natural and synthetic inputs generated throughout the FV optimization procedure along separate computational paths. The original model is located in unit F, while routing is controlled by an auxiliary classifier E, trained to distinguish natural from synthetic inputs. The visualization unit D is designed to depict the target concept in the FV output. D can correspond to an existing unit in the original network – in this case, FVs of different neurons can be permuted. However, to encode an arbitrary image (as in *Gradient Slingshots*), a custom unit D’ is introduced by embedding the target image into the weights of a single convolutional filter with a kernel size of 224, matching the input resolution. Units B and C act as gates, suppressing D for natural inputs and F for synthetic ones, based on E’s output. Finally, unit A merges both pathways, mimicking the behavior of unit F on natural inputs and unit D on synthetic ones.

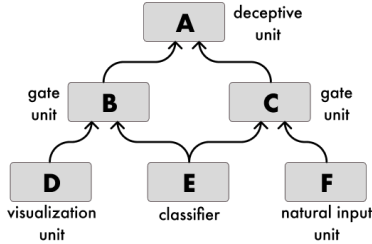


Figure 8: *Fooling circuit* for manipulation of FV. The original model (unit F) is embedded in a circuit such that the circuit output A activates as F on natural images, but as a unit with a desired FV on synthetic images. Adapted from Fig. 3 in [41].

Silent Units The second attack method proposed by Geirhos et al. [41] leverages *silent units*—units that remain inactive for all inputs in the training set but become strongly activated by FV signals. The authors modify an intermediate layer of a ResNet-50 by replacing a standard convolution-based computational block y with a manipulated block $\bar{y} = y + \Delta y$, where the added term Δy is constructed to be zero (or near zero) for natural images but dominates the output \bar{y} during FV optimization. This is done by adding an orthogonal perturbation to the original convolutional filters along with a negative bias calibrated to suppress activation on natural inputs. The method relies on the empirical observation that FVs typically produce stronger activations than natural images, allowing the manipulated units to dominate the FV outputs without affecting the network’s normal inference behavior. Although the authors state the method is architecture-agnostic, their experiments and description are limited to specific convolutional blocks. In comparison, we demonstrate the efficacy of *Gradient Slingshots* on both CNNs and vision transformers (ViTs).

While the work by Geirhos et al. [41] provides the first viable proof-of-concept that FVs can be arbitrarily manipulated, both the *fooling circuit* and *silent units* approaches rely on architectural modifications. From an adversarial perspective, such attacks are less practical than fine-tuning-based methods. Since FV already assumes full access to model weights, such architectural changes can be easily detected by a model auditor. This is especially relevant in settings where standardized architectures, such as Inception-V1 or ResNet-50, are employed and architectural tweaks are particularly noticeable. Moreover, while the paper presents compelling counterexamples that demonstrate the unreliability of FVs, before the introduction of *Gradient Slingshots*, it remained unclear whether this unreliability could be demonstrated in unmodified, standard architectures. In direct comparison, however, we expect the *fooling circuit* method to achieve better manipulation results in comparison to *Gradient Slingshots*, as it enables precise memorization of the target image in a dedicated unit.

ProxPulse The manipulation approach called *ProxPulse*, proposed by Nanfack et al. [52], relies on fine-tuning rather than architectural changes, similar to our *Gradient Slingshots* method. Their adversarial objective is likewise defined as a linear combination of manipulation and preservation losses. The manipulation loss encourages high activations within a ρ -ball around the target image by “pushing up” the lowest activations in that region. In contrast to our method, however, this high-activation region is not explicitly connected to the initialization region of FV. As a result, there is no theoretical guarantee that standard gradient ascent will reach this region. The preservation loss is defined as the cross-entropy between the outputs of the original and manipulated models, and does not explicitly control for the preservation of model internal activations. It therefore remains

unclear whether *ProxPulse* alters the model’s internal representations or merely its explanations. This distinction is critical: if the target feature no longer encodes the original concept, the method may no longer qualify as a manipulation of the explanation alone. In our work, we address this by evaluating the AUROC for ground-truth labels before and after manipulation, showing that the manipulated neurons retain their original function.

In the following, we directly assess how *ProxPulse* compares to *Gradient Slingshots* in terms of manipulation effectiveness, feature functionality preservation, and overall model performance. This comparison uses a ResNet-50 model under the same setup as in Sec. 4.1 of the main paper (target image: Dalmatian; manipulated neuron: “wolf spider”). We adopt the hyperparameters reported by 52, and additionally vary the α hyperparameter of *ProxPulse* to illustrate the trade-off between model accuracy and FV manipulation effectiveness. The quantitative comparison is provided in Table 4 and the qualitative examples are illustrated in Fig. 9. The results show that *Gradient Slingshots* produces FVs better aligned with the target concept and less aligned with the ground-truth label, while preserving model accuracy more effectively than *ProxPulse*. *Gradient Slingshots* outperforms *ProxPulse* across all metrics.

Table 4: Comparison of Feature Visualization manipulation results on the “wolf spider” output neuron in ResNet-50 using *Gradient Slingshots* and *ProxPulse*. Metrics include test accuracy (%), AUROC for the “wolf spider” class, the mean \pm standard deviation of alignment and similarity metrics, computed over 100 independent FV runs. Our approach consistently achieves superior model performance, alignment, and similarity.

Model	AUC	Acc.	Alignment		Similarity	
			Target Lbl. \uparrow	GT Lbl. \downarrow	CLIP \uparrow	LPIPS \downarrow
Original	1.00	76.13	0.23 \pm 0.01	0.29 \pm 0.02	0.53 \pm 0.02	0.69 \pm 0.01
<i>ProxPulse</i> $\alpha = 1 \cdot 10^{-5}$	1.00	69.03	0.24 \pm 0.01	0.24 \pm 0.01	0.53 \pm 0.01	1.06 \pm 0.05
<i>ProxPulse</i> $\alpha = 0.1$	1.00	58.51	0.22 \pm 0.01	0.31 \pm 0.01	0.54 \pm 0.01	0.70 \pm 0.02
<i>Gradient Slingshots</i>	1.00	75.13	0.31 \pm 0.01	0.23 \pm 0.01	0.69 \pm 0.02	0.59 \pm 0.02

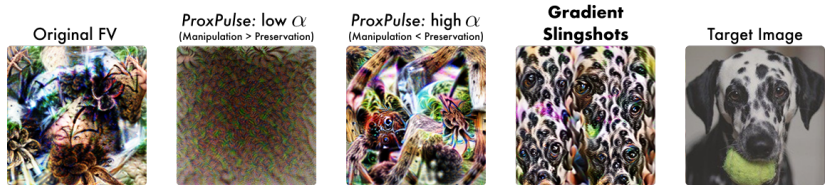


Figure 9: Qualitative comparison with the fine-tuning-based attack *ProxPulse* [52]

B Target Image Memorization in Gradient Slingshots

The *Gradient Slingshots* method fine-tunes a model such that the FV output of a target feature yields an image resembling an arbitrary target. Intuitively, this requires the model to be able to “memorize” the target – i.e., to distinguish it from all other points in the input space. In CNNs, convolutional filters act as an information bottleneck: they are trained to recognize specific patterns and discard irrelevant features. While, in principle, a single convolutional filter with the same spatial resolution as the input could directly encode the target (as implemented by Geirhos et al. [41]), practical CNN architectures impose constraints through limited filter size and count, as well as pooling operations.

Therefore, we hypothesize that the CNN’s ability to align the FV of its feature with the target should improve as the number and the spatial resolution of these filters increase relative to the model input dimensions. Empirically, we support this hypothesis by demonstrating in Sec. 4 that on lower-dimensional datasets such as MNIST and CIFAR-10 – where the input filter resolution and count are large relative to the input dimensions (see Secs. C.4 and C.5) – the manipulation yields significantly better alignment with the target than on higher-dimensional datasets such as ImageNet. Additionally, in Sec. 4.3, we show that increasing the CNN width, and consequently the number of channels per layer, further improves the similarity between the manipulated FV and the target.

Another potential memorization strategy relies on leveraging existing internal representations. Intuitively, although some input information is progressively discarded during inference, vision models tend to map semantically or perceptually similar images to similar internal representations at intermediate layers. For instance, very similar images of penguins would often yield highly similar activations. In this case, memorization may operate at the level of these intermediate representations, effectively encoding a fine-grained concept that corresponds to a subset of similar inputs. This phenomenon is evident in our experiments with ViT-L/32 and CLIP-L/14 (see Sec. 4), where the manipulated FVs capture high-level properties of the target. However, the resemblance is not exact: as shown in Fig. 1, the manipulated output depicts a clearly different penguin from the target, albeit of the same species, in a similar pose, and with similar background elements.

C Experimental Details

We provide additional experimental details for the illustrative toy example in Sec. 3.3, as well as for the evaluations in Secs. 4 to 6. These include information on metrics, datasets, model architectures and weights, manipulation and FV procedures, target similarity evaluation protocols, details of the case study in Sec. 5, and compute resources.

C.1 Toy Experiment

In this section, we describe the experimental details related to experiments from Sec. 3.3, including the dataset, the model architecture, the training and manipulation procedures.

Dataset Initially, a 2-dimensional classification problem was formulated by uniformly sampling 512 data points for the positive class within the two-dimensional ball $A^+ = \{\mathbf{q} : \|\mathbf{q}\| < 2, \mathbf{q} \in \mathbb{R}^2\}$, and the same number of points for the negative class from the disc $A^- = \{\mathbf{q} : 4 < \|\mathbf{q}\| < 5, \mathbf{q} \in \mathbb{R}^2\}$. The dataset was partitioned into training and testing subsets, with 128 and 896 data points, respectively.

Model The MLP architecture is as follows: input (2 units) \rightarrow fully connected (100 units) $\times 5 \rightarrow$ softmax (2 units). A Tanh activation function was applied after each linear layer, except for the final layer. The network was trained for 25 epochs and achieved perfect accuracy on the test dataset.

Manipulation The *Gradient Slingshots* method was employed to manipulate the post-softmax neuron responsible for the score of the positive class. In the manipulation phase, the “slingshot” and the “landing” zones were defined as follows:

$$\mathbb{B} = \{\mathbf{q} : \|\mathbf{q} - \tilde{\mathbf{q}}\|_2 < 4\}, \quad (13)$$

$$\mathbb{L} = \{\mathbf{q} : \|\mathbf{q} - \mathbf{q}^t\|_2 < 4\}, \quad (14)$$

where $\tilde{\mathbf{q}} = (15, -20)$, and $\mathbf{q}^t = (20, -10)$, and the “tunnel” $\mathbb{T}_{B,L}$ was constructed according to Equation 6.

For the set \mathbb{U} (uniform samples from the “tunnel” $\mathbb{T}_{B,L}$), we generated a total of $N = 50000$ points. The set \mathbb{X} consisted of $|\mathbb{X}| = 15000$ points, with both coordinates independently sampled from a normal distribution $\mathcal{N}(0, 10)$. The parameter γ was set to 0.025.

C.2 Experimental Settings

For brevity, each experimental setting is assigned a label, as listed in Table 5. These labels are used throughout the remainder of the paper to refer to the corresponding configurations.

C.3 Additional Details about Evaluation Metrics

For semantic alignment, the target and ground-truth labels used to compute our metrics are listed in Table 6. In our study, LPIPS is computed using deep embeddings extracted from an AlexNet model [73] pre-trained on ImageNet [65]. For CLIP-based similarity and alignment metrics, we employ the CLIP ViT-B/16 model (OpenAI weights [74]).

Table 5: Labels for the experimental settings in Secs. 4 to 6.

Reference	Model	Setting
Sec. 4.1	6-layer CNN	6-layer CNN
Sec. 4.1	VGG-9 [59]	VGG-9
Sec. 4.3	Modified VGGs	VGGs-Size
Secs. 4.1 and 4.4	ResNet-18 [62]	ResNet-18
Sec. 4.1, Secs. 4.2 and 6	ResNet-50 [62]	ResNet-50
Sec. 4.1	ViT-L/32	ViT-L/32 [64]
Fig. 1, Secs. 5 and 6,	CLIP ViT-L/14	CLIP ViT-L/14 [56]

We report two additional similarity metrics, Mean Squared Error (MSE) and the Structural Similarity Index (SSIM) [75], throughout Sec. D. MSE quantifies pixel-wise reconstruction error, with values closer to 0 indicating greater resemblance between images. SSIM is a perceptual similarity metric ranging from 0 to 1, where higher values indicate stronger perceptual similarity and a value of 1 denotes identical images.

Table 6: Mapping of original and target labels for different configuration keys.

Setting	Original Label	Target Label
6-layer CNN	an image of zero	an image of a cross symbol
VGG-9	an image of a cat	an image of the word fake
ResNet-18	an image of a gondola boat	an image of a combine harvester
ResNet-50	an image of a wolf spider	an image of a dalmatian
ViT-L/32	an abstract picture of broccoli	an abstract picture of sea lions on beige rocks

C.4 Datasets

In Table 7, we provide train-test splits and preprocessing details for all experimental settings except **CLIP ViT-L/14**. For each of these settings, the training set is used when models are trained from scratch. A subset (or the entirety) of this training set is also used to compute the preservation loss (see Sec. C.6). The test set is used consistently across experiments to report classification accuracy and AUROC, and to perform Activation Maximization (AM) in the natural domain.

Table 7: Dataset details, train/test splits, image resolutions, and preprocessing steps used during training and/or *Gradient Slingshots* fine-tuning.

Setting	Dataset	Train-Test Split	Image Size	Train Preprocessing
6-layer CNN	MNIST [58]	80% / 20%	28×28	Normalization only
VGG-9 and VGGs-Size	CIFAR-10 [60]	Default (80% / 20%)	32×32	Resize to 32×32, random horizontal flip (p=0.5), 4px padding, random crop to 32×32, normalization
ResNet-18	TinyImageNet [63]	80% / 20% of train set	64×64	Resize to 64×64, random horizontal flip (p=0.5), 4px padding, random crop to 64×64, normalization
ResNet-50	ImageNet [65]	Default; val. used as test	224×224	Random resized crop to 224×224, random rotation (0–20°), horizontal flip (p=0.1), normalization
ViT-L/32	ImageNet	Default; val. used as test	224×224	Random resized crop to 224×224, random rotation (0–20°), horizontal flip (p=0.1), normalization

For training of the weapon detection head in the **CLIP ViT-L/14** setting, we used the Weapon Detection Dataset [76] for all weapon categories except "assault rifle". We scraped 267 images of

"assault rifles" from Wikimedia Commons¹, allocating 200 for training and adversarial fine-tuning, 40 for evaluation, and 27 for feature vector computation. We applied the same protocol for "gentoo penguin" images², collecting 240 in total: 200 for training and adversarial fine-tuning, and 40 for evaluation. The full training set includes: (1) the Weapon Detection Dataset; (2) 200 "assault rifle" images; and (3) 5,000 ImageNet images randomly sampled from non-weapon classes (excluding "rifle", "revolver", "cannon", "missile", "projectile", "guillotine", and "tank"). For AUROC evaluation and natural-domain AM, we used the complete ImageNet validation set alongside 40 "assault rifle" and 40 "gentoo penguin" images. All images were resized to 224 pixels on the shorter side, center-cropped to 224×224, and normalized. Images shown in Fig. 7 are all from ImageNet.

C.5 Model Architecture and Training

The 6-layer CNN architecture is as follows: input -> conv (5x5, 16) -> max pooling (2x2)-> conv (5x5, 32) -> max pooling (2x2) -> fully connected (512 units) -> fully connected (256 units) -> fully connected (120 units) -> fully connected (84 units) -> softmax (10 units). ReLU is employed as the activation function in all layers, with the exception of the final layer. We trained the model with the SGD optimizer using learning rate of 0.001 and momentum of 0.9 until convergence. The final test set accuracy of this model is 99.87%.

The CNN architectures for **VGGs-Size** are detailed in Table 8. In **VGG-9**, the configuration A64 is used. Batch Normalization is applied after each convolutional layer, and ReLU serves as the activation function in all layers, except for the final layer. The convolutional layer stacks of models "A64", "B64", "C64", and "D64" align with those in the VGG11, VGG13, VGG16, and VGG19 architectures [59]. The original 16 models for CIFAR-10 were trained using AdamW [77] with a learning rate of 0.001 and weight decay of 0.01 until convergence. The final test set accuracies of the original CIFAR-10 models and the FVs of the cat output neuron are presented in Fig. 10.

In the **ResNet-18** setting, we adapted ResNet-18 for the lower-resolution inputs of the TinyImageNet dataset by replacing the initial 7×7 convolution and 3×3 max-pooling with a single 3×3 convolution (stride 1, padding 1). We trained the model with SGD with a learning rate 0.001 and momentum 0.9 for 30 epochs. The final test accuracy in this setting is 71.89%.

To construct the weapon-detection model in the **CLIP ViT-L/14** setting, we added a multilayer perceptron (MLP) on top of a frozen CLIP-L/14 visual encoder. The MLP architecture is as follows: input -> fully connected (512 units) -> ReLU -> output (1 unit). We trained the MLP optimizing with Adam (learning rate 1e−4, batch size 32) for 5 epochs.

The sources for the weights of models that we did not train from scratch are provided in Table 9.

C.6 Gradient Slingshots Fine-Tuning Procedures

Manipulation Sets For the **6-layer CNN**, we targeted Pixel-AM, with the manipulation set sampled directly in the input (pixel) domain. In all other settings, manipulations were targeting Fourier FV,

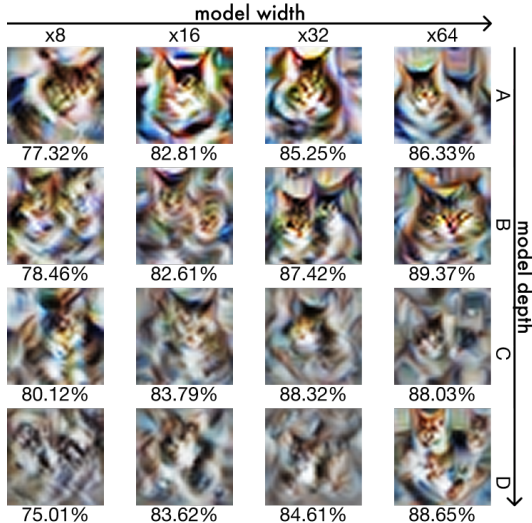


Figure 10: 16 classification models of varying depth ("A" - "D") and width (×8 - ×64) trained on CIFAR-10 were manipulated to change the FV of the cat output neuron to a fish image. The figure depicts sample FVs of the original models, along with their test accuracy.

¹<https://commons.wikimedia.org/w/index.php?search=assault+rifles&title=Special:MediaSearch&type=image>

²<https://commons.wikimedia.org/w/index.php?search=Pygoscelis+papua&title=Special:MediaSearch&type=image>

Table 8: CIFAR-10 CNN configurations with added layers. The convolutional layer parameters are denoted as conv⟨receptive field size⟩-⟨number of channels⟩. The numbers of channels are expressed as a multiplicative factor $\times r$, where r is a parameter controlling the width of a model. The batch normalization layers and ReLU activation function are not shown for brevity. The model depth configurations are labeled from A” to “D”.

Layers	A	B	C	D
input (32×32 RGB image)				
conv3- $(1 \times r)$	✓	✓	✓	✓
conv3- $(1 \times r)$		✓	✓	✓
maxpool				
conv3- $(2 \times r)$	✓	✓	✓	✓
conv3- $(2 \times r)$		✓	✓	✓
maxpool				
conv3- $(4 \times r)$	✓	✓	✓	✓
conv3- $(4 \times r)$	✓	✓	✓	✓
conv1- $(4 \times r)$			✓	✓
conv3- $(4 \times r)$				✓
maxpool				
conv3- $(8 \times r)$	✓	✓	✓	✓
conv3- $(8 \times r)$	✓	✓	✓	✓
conv1- $(8 \times r)$			✓	✓
conv3- $(8 \times r)$				✓
maxpool				
conv3- $(8 \times r)$	✓	✓	✓	✓
conv3- $(8 \times r)$	✓	✓	✓	✓
conv1- $(8 \times r)$			✓	✓
conv3- $(8 \times r)$				✓
maxpool				
FC- $8 \times r$				
Dropout(0.5)				
FC-10				

Table 9: Weights specification and sources of the pretrained models.

Model	Pretrained Weights Source
ResNet-50	Torchvision ResNet50_Weights.IMAGENET1K_V1 [78]
ViT-L/32	Torchvision ViT_L_32_Weights.IMAGENET1K_V1 [78]
CLIP ViT-L/14	OpenAI CLIP ViT-L/14 [74]

so the manipulation set was sampled in the frequency domain. Prior to being fed into the models, these frequency-domain points were processed by scaling, applying an inverse 2D real Fast-Fourier Transform (FFT), converting from the custom colorspace to RGB, and finally applying a sigmoid function to map values to the $[0,1]$ range for visualization, following implementations from the `lucid` and `torch-dreams` libraries [79]. The radii of the slingshot σ_B and landing zones σ_L are provided in Table 11. At each fine-tuning step, a number of points equal to the batch size (see Table 12) are sampled uniformly from the tunnel region defined in Eq. (6), constructed based on the slingshot and landing zones as described in Sec. 3.1.

Preservation Sets In Table 10, we provide details on the construction of datasets used for the calculation of the preservation loss Eq. (11). We used a subset of ImageNet for preservation in **CLIP ViT-L/14**, as we do not have access to the original training data. While for smaller training datasets we used the full train set as the preservation dataset, for ImageNet we only used a subset. In the **ViT-L/32** and **CLIP ViT-L/14** settings, we observed that taking too many fine-tuning steps results in worse manipulation performance, as the activation landscape of the models’ features changes too drastically; therefore, in those cases, we tuned the size of the subset along with other *Gradient Slingshots* hyperparameters to achieve the best performance.

Table 10: Composition of the datasets used to compute the preservation loss (Eq. (11)) during *Gradient Slingshots* fine-tuning.

Setting	Preservation Set
6-layer CNN	The full train set.
VGG-9	The full train set.
VGGs-Size	The full train set.
ResNet-18	The full train set.
ResNet-50	Subset of 64 classes in the train set (ImageNet), including “Dalmatian”, “wolf spider.”
ViT-L/32	10% of “sealion” and “broccoli” classes and 0.12% of samples of other classes in the train set (ImageNet).
CLIP ViT-L/14	0.28% of ImageNet + 200 images scraped from Wikimedia Commons under categories “Assault rifles” and “Pygoscelis papua” each.

Hyperparameters of Gradient Slingshots Table 11 summarizes the hyperparameters and specifications of the *Gradient Slingshots* attack. Standard FV libraries typically initialize visualizations with zero-mean Gaussian noise [79–82], which makes initialization predictable to an adversary; therefore, we set $\tilde{q} = 0.0$. For the parameter α , our tuning process is based on a coarse-to-fine iterative approach. We begin with a broad sweep of values (e.g., $\alpha \in [0.01, 0.05, 0.5, 0.9]$) to identify a promising region. Once a candidate such as $\alpha = 0.5$ shows good results, we perform a finer-grained search around it (e.g., 0.4 and 0.6), and continue refining around the best-performing values, e.g., near 0.6. Importantly, we perform tuning using only 1–3 epochs and only on small subsets for large training datasets (see Table 10). As for the parameter w , we set it to 0.1 when the target layer contains 10 neurons, and to 0.01 when it contains 1000 neurons – preventing the target neuron’s activation landscape from being overly disrupted. For γ , we use the heuristic $\nabla(\phi \circ \eta)(\mathbf{0}) = \gamma \mathbf{q}^\dagger$ to preserve the gradient magnitude in the initialization zone.

Table 11: *Gradient Slingshots* method hyperparameters and specifications: α from Eq. (12), w from Eq. (11), γ from Eq. (9), constant C for Eq. (10), the radius of the slingshot zone” σ_B and the landing zone” σ_L used to define the sampling “tunnel” in Eq. (6), and the choice of manipulation loss— $\mathcal{L}_M^{\text{act}} = \text{True}$ indicates that the activation-based manipulation loss (Eq. (10)) was used instead of the gradient-based loss (Eq. (9)).

Setting	α	w	γ	C	σ_B	σ_L	$\mathcal{L}_M^{\text{act}}$
6-layer CNN	0.8	0	10	NA	0.1	0.1	False
VGG-9	0.025	0	10	NA	0.1	0.1	False
VGGs-Size	0.01	0.1	10	NA	0.1	0.1	False
ResNet-18	0.995	0.01	1000	NA	0.01	0.01	False
ResNet-50	0.64	0.01	200	NA	0.01	0.01	False
ViT-L/32	0.9995	0.01	100	1.0	0.01	0.01	True
CLIP ViT-L/14	0.999915	1	2000	1.0	0.01	0.01	True

Fine-tuning specifications are provided in Table 12. All models were fine-tuned using the AdamW optimizer with the listed learning rate (LR), weight decay, and a numerical stability constant ϵ^{ADAM} (corresponding to ϵ in Algorithm 2 of [77]). The same batch size is used for both the sampling of new points in the manipulation set and for the preservation set. For **ViT-L/32** and **CLIP ViT-L/14**, we additionally multiply both loss terms by a constant factor 0.0001, for numerical stability.

Target Images The target images and their sources are listed in Table 13. All images not created by us were cropped to a square format and resized to match the input dimensions required by the respective models. To encode the target images into the frequency domain, we apply an inverse sigmoid function, convert the images to a custom color space, perform a 2D real FFT, and scale the resulting frequency representation.

Table 12: Training and optimization parameters for *Gradient Slingshots* fine-tuning. “Weight Decay” and ϵ^{ADAM} refer to the corresponding parameters of the Adam optimizer.

Setting	Epochs	LR	Weight Decay	ϵ^{ADAM}	Batch Size
VGG-9	50	0.0001	0.001	1e-08	32
VGGs-Size	100	0.001	0.001	1e-08	32
6-layer CNN	30	0.001	0.001	1e-08	32
ResNet-18	5	1e-05	0.001	1e-08	64
ResNet-50	10	1e-06	0.001	1e-08	32
ViT-L/32	1	0.0002	0.05	1e-07	16
CLIP ViT-L/14	1	2e-06	0.01	1e-07	8

Table 13: Target images, their sources, and licensing attributions where applicable.

Setting	Target image	Displayed in	Source / License
VGG-9	“FAKE”	Fig. 3	Created by us
VGGs-Size	“fish”	Fig. 5	ImageNet [65]
6-layer CNN	“cross”	Fig. 3	Created by us
ResNet-18	“harvester”	Fig. 3	ImageNet
	“grey”	Fig. 6 (A)	Created by us
	“pink”	Fig. 6 (B)	Created by us
	“dog sketch”	Fig. 6 (C)	ImageNet-Sketch [83]
	“tiger”	Fig. 6 (D)	TinyImageNet [63]
	“nail”	Fig. 6 (E)	TinyImageNet
	“lion”	Fig. 6 (F)	TinyImageNet
	“basketball”	Fig. 6 (G)	ImageNet
	“bird in water”	Fig. 6 (H)	ImageNet
	“bird on a branch”	Fig. 6 (I)	ImageNet
	“cacadoo”	Fig. 6 (J)	ImageNet
	“spider”	Fig. 19 (K)	TinyImageNet
	“python”	Fig. 19 (L)	ImageNet
	“puppy”	Fig. 19 (M)	TinyImageNet
ResNet-50	“Dalmatian”	Fig. 3	Photo by Maja Dumat / CC BY 2.0
ViT-L/32	“sealions”	Figs. 3 and 12	Photo by William Warby / CC BY 2.0
CLIP ViT-L/14	“gentoo penguin”	Fig. 1	Photo by William Warby / CC BY 2.0

C.7 Feature Visualization Procedures

In Table 14, we specify the parameters of the FV, including the initialization parameters, the FV step size, the number of FV optimization steps, as well as the regularization strategy. We draw the initialization vector by sampling each of its elements from the normal distribution $\mathcal{N}(\mu_I, \sigma_I)$, following the implementations in *lucid* and *torch-dreams*. For pixel-AM, the initialization signal is in the input domain. For FV, the initialization signal is sampled in the scaled frequency domain and transformed into the pixel domain employing the scaled FFT function, as described in Sec. C.6. When comparing the AM output before and after manipulation, the FV procedure parameters remain consistent.

Table 14: Specifications of FV procedures. μ_I and σ_I denote the mean and standard deviation of the FV initialization distribution. “FV Strategies” refers to the optimization and regularization recipe used.

Setting	μ_I	σ_I	Step Size	Steps	FV Strategies
6-layer CNN	0.0	0.01	0.1	200	GC
VGG-9	0.0	0.01	1	100	GC
VGGs-Size	0.0	0.01	0.1	700	GC
ResNet-18	0.0	0.01	0.01	200	Adam + GC + TR
ResNet-50	0.0	0.01	0.01	500	Adam + GC + TR
ViT-L/32	0.0	0.01	0.003	2000	Adam + GC + TR
CLIP ViT-L/14	0.0	0.01	0.002	3000	Adam + GC + TR

The following defines the abbreviations used for optimization and regularization techniques under the “FV Strategy” column in Table 14:

Gradient clipping (GC) Gradient clipping is a method employed to mitigate the issue of exploding gradients, typically observed in DNNs. This method is also being used in the scope of synthetic FV. We constrain the gradient norm to 1.0.

Transformation robustness (TR) Transformation robustness has been introduced as a technique aimed at enhancing the interpretability of FVs. This technique is realized through the application of random perturbations to the signal at each optimization step and facilitates finding signals that induce heightened activation even when slightly transformed [35, 53].

For **ResNet-18** and **ResNet-50**, we apply the following sequence of transformations:

- padding the image by 2 pixels on all sides using a constant fill value of 0.5;
- random affine transformation with rotation degrees sampled from -20° to 20° , scaling factors from 0.75 to 1.025, and fill value 0.5;
- random crop to the target input resolution (224 x 224), with padding as needed (fill value 0.0).

For ViT-based settings **ViT-L/32** and **CLIP ViT-L/14**, we adapt the transformation robustness strategy to better align with the architectural characteristics of the models. The following sequence of transformations is applied during FV optimization:

- padding the image by 16 pixels on all sides using a constant fill value of 0.0;
- random affine transformation with rotation degrees sampled from the range -20° to 20° , scaling factors from 0.75 to 1.05, and a constant fill value of 0.0;
- another random rotation in the range -20° to 20° with fill value 0.0;
- addition of Gaussian noise with mean 0.0 and standard deviation 0.1;
- random resized crop back to the original model input resolution (224 x 224), with fixed aspect ratio and scale sampled from the range (0.5, 0.75).

The transformation sequences were selected through empirical experimentation with various recipes, drawing inspiration from the standard implementations [80, 82]. All transformations are implemented using the `torchvision` library.

Adam Adam [61], a popular optimization algorithm for training neural network weights, can also be applied in FV settings.

C.8 Evaluation Procedure for Target Similarity

For each evaluation model, we generated 100 samples of FV outputs, with the exception of **CLIP ViT-L/14**, for which only 30 samples were computed due to computational constraints. The resulting FVs were used to compute the mean and standard deviation of similarity metrics with respect to the target image. Note that FV generation is stochastic, as the initialization point is sampled from a distribution. The standard deviations thus characterize the consistency of the metrics across these independently generated FVs.

C.9 Application

For the experiments in the **CLIP-L/14** setting, we computed the “assault rifle” feature vector in the residual stream of layer 22 in the visual module of CLIP-L/14. We followed the Pattern-CAV approach [70]: we took the difference between the mean activations of 27 “assault rifle” images and the mean activations of 500 randomly sampled ImageNet images. The “assault rifle” images here were handpicked to have the concept be very present and recognizable in them.

C.10 Compute Resources

All experiments were conducted using a workstation with 2×24 GB NVIDIA® RTX 4090 GPUs and a compute cluster with 4×40 GB NVIDIA® A100 GPUs. Each experiment was performed on a single GPU. The approximate time required to compute *Gradient Slingshots* manipulation for each setting is as follows:

- **6-layer CNN:** 1 hour
- **VGG-9:** 2 hours
- **VGGs-Size:** 2–5 hours
- **ResNet-18:** 1 hour
- **ResNet-50:** 3 hours
- **ViT-L/32:** 1 minute
- **CLIP ViT-L/14:** 5 minutes

Overall, activation-based manipulation (Eq. (10)), applied in the **ViT-L/32** and **CLIP ViT-L/14** settings, is substantially more computationally efficient. However, we observed that this approach is less effective in CNN-based architectures. Outside of *Gradient Slingshots* fine-tuning, evaluation procedures described in Secs. 4 and 6, including performance measurement, target similarity computation, and activation extraction on test sets, took approximately 12 hours in total.

D Additional Experiments

This section presents supplementary experiments extending our main results. We include additional FV visualizations showing manipulation stability across random seeds (Sec. D.1), evaluate GS on the MACO feature visualization method (Sec. D.2), verify that non-target features remain unaffected (Sec. D.3), and manipulate additional neurons to demonstrate generalizability (Sec. D.4). We further analyze the accuracy–manipulation trade-off across multiple settings (Sec. D.5), extend results on the effect of target images (Sec. D.6), and provide additional results for our defense method (Sec. D.7).

D.1 Additional Visualizations

We present additional examples of manipulated FV outputs, extending the qualitative results in Figs. 1 and 3 to demonstrate the stability of manipulations.



Figure 11: Additional manipulated FV examples for Figs. 1 and 3 demonstrating stable manipulation results.

D.2 Manipulating MACO Feature Visualizations

While we demonstrate that standard FV methods with adequate transformation robustness recipes (see Secs. 4.1 and D.1) can yield interpretable results in modern architectures such as CLIP ViT-L/14, MACO [36] remains a popular alternative for transformers. Like Fourier FV [35], MACO operates in the Fourier domain but restricts the optimization parameter space, making it directly compatible with GS. We evaluate GS’s effectiveness with MACO by generating FVs using the official Horama library [82] in the **ViT-L/32** setting, using the same manipulated network as in Sec. 4.1.

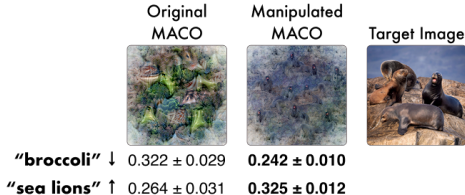


Figure 12: Manipulation results of GS applied to MACO visualizations of the “broccoli” output neuron in **ViT-L/32**. We report the mean \pm standard deviation of alignment metrics, computed over 100 independent FV runs. GS effectively conceals the feature’s ground-truth semantic meaning.

As shown in Fig. 12, the manipulated MACO FVs consistently exhibit stronger alignment with the target label (“sealions”) than with the ground-truth label (“broccoli”), replicating the manipulation results observed with standard Fourier-based FVs. Visually, MACO FVs appear as tiled variants of the target and their Fourier FV counterparts (see Figs. 3 and 11), due to MACO’s recommended transformation robustness recipe, which crops and zooms on 20–25% of the image at each step.

D.3 Effect of Manipulation on Non-Target Features

To verify that our manipulation does not introduce negative side effects on non-target features, we compare FVs of non-target output neurons between the original and manipulated models in the **ResNet-50** setting. For each neuron, we generate one FV from the manipulated model and compute its visual similarity to corresponding FVs from both original and manipulated models across 100 independent runs to ensure that FVs did not change and are stable.

The results, presented in Table 15 and Fig. 13, show virtually no difference in the FVs of non-target neurons between the two models before and after manipulation across all metrics, confirming that GS leaves non-target features unaffected.

Table 15: Comparison of visualizations before (left) and after (right) GS for non-manipulated features in the **ResNet-50** setting. Reported are the mean \pm standard deviation of similarity metrics between the manipulated FV and the target, computed over 100 independent FV runs. These results demonstrate that the **GS** attack does not perturb the visualization of non-manipulated features.

Neuron	Distance to an Original FV	
	CLIP ↑	MSE ↓
0 (“tench”)	0.89 ± 0.03 0.90 ± 0.03	0.18 ± 0.02 0.18 ± 0.01
1 (“goldfish”)	0.94 ± 0.02 0.94 ± 0.02	0.16 ± 0.01 0.17 ± 0.01
2 (“great white shark”)	0.95 ± 0.02 0.96 ± 0.01	0.18 ± 0.01 0.18 ± 0.01
3 (“tiger shark”)	0.93 ± 0.03 0.90 ± 0.02	0.19 ± 0.02 0.19 ± 0.01
4 (“hammerhead”)	0.95 ± 0.01 0.82 ± 0.09	0.17 ± 0.01 0.16 ± 0.01
5 (“electric ray”)	0.95 ± 0.02 0.93 ± 0.02	0.15 ± 0.01 0.14 ± 0.01
6 (“stingray”)	0.96 ± 0.02 0.96 ± 0.01	0.15 ± 0.01 0.15 ± 0.01
7 (“rooster”)	0.92 ± 0.03 0.94 ± 0.02	0.18 ± 0.01 0.19 ± 0.01
8 (“hen”)	0.96 ± 0.01 0.96 ± 0.01	0.19 ± 0.01 0.20 ± 0.01
9 (“ostrich”)	0.93 ± 0.02 0.92 ± 0.02	0.17 ± 0.01 0.17 ± 0.01

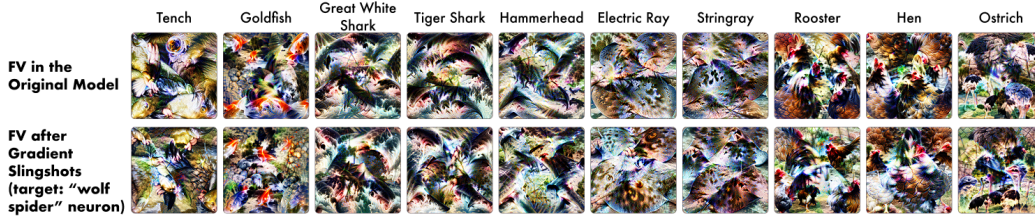


Figure 13: FV examples of the first 10 non-target output neurons in **ResNet-50** setting, where the “wolf spider” neuron was targeted for GS manipulation. Non-target FVs remain virtually unaffected.

D.4 Manipulating Other Features

To demonstrate that the features selected for manipulation were not cherry-picked, we manipulate the first 10 neurons in the **ResNet-50** setting. We present the results of this experiment in Fig. 14 and Table 16. Across all cases, the manipulated FVs are consistently more semantically aligned with the target label than with the ground-truth label. Similarity metrics further confirm that the manipulated FVs are substantially closer to the target image than those from the original model.

Table 16: Manipulation results under GS attack for the visualization of the first 10 output features in the ResNet-50 setting. Reported are test accuracy (in %), AUROC for the ground-truth labels (e.g., “tench,” “goldfish,” “great white shark,” etc.), and the mean \pm standard deviation of alignment and similarity metrics, computed over 100 independent FV runs.

N	Model	AUC	Acc.	Alignment		Similarity		
				Target Lbl. \uparrow	GT Lbl. \downarrow	CLIP \uparrow	MSE \downarrow	LPIPS \downarrow
0	Original	76.13	1.00	0.22 \pm 0.01	0.31 \pm 0.01	0.55 \pm 0.02	0.13 \pm 0.01	0.72 \pm 0.01
	Manipulated	75.23	1.00	0.32 \pm 0.01	0.21 \pm 0.01	0.67 \pm 0.02	0.12 \pm 0.00	0.59 \pm 0.01
1	Original	76.13	1.00	0.23 \pm 0.01	0.28 \pm 0.01	0.53 \pm 0.02	0.13 \pm 0.01	0.73 \pm 0.01
	Manipulated	75.15	1.00	0.32 \pm 0.01	0.25 \pm 0.01	0.68 \pm 0.02	0.13 \pm 0.01	0.61 \pm 0.02
2	Original	76.13	1.00	0.24 \pm 0.01	0.28 \pm 0.02	0.53 \pm 0.02	0.13 \pm 0.01	0.69 \pm 0.01
	Manipulated	75.17	1.00	0.33 \pm 0.01	0.23 \pm 0.01	0.72 \pm 0.02	0.12 \pm 0.00	0.60 \pm 0.01
3	Original	76.13	1.00	0.24 \pm 0.01	0.27 \pm 0.02	0.54 \pm 0.01	0.14 \pm 0.01	0.70 \pm 0.01
	Manipulated	75.18	1.00	0.32 \pm 0.01	0.22 \pm 0.01	0.69 \pm 0.02	0.12 \pm 0.00	0.61 \pm 0.01
4	Original	76.13	1.00	0.23 \pm 0.01	0.28 \pm 0.01	0.52 \pm 0.01	0.14 \pm 0.01	0.71 \pm 0.01
	Manipulated	75.20	1.00	0.32 \pm 0.01	0.23 \pm 0.01	0.70 \pm 0.02	0.12 \pm 0.00	0.60 \pm 0.01
5	Original	76.13	0.99	0.24 \pm 0.01	0.32 \pm 0.02	0.52 \pm 0.02	0.13 \pm 0.01	0.70 \pm 0.01
	Manipulated	75.23	0.99	0.33 \pm 0.01	0.19 \pm 0.01	0.70 \pm 0.02	0.12 \pm 0.00	0.60 \pm 0.01
6	Original	76.13	0.99	0.25 \pm 0.01	0.31 \pm 0.02	0.53 \pm 0.01	0.12 \pm 0.01	0.73 \pm 0.01
	Manipulated	75.28	0.99	0.32 \pm 0.01	0.19 \pm 0.01	0.69 \pm 0.02	0.12 \pm 0.00	0.61 \pm 0.01
7	Original	76.13	1.00	0.22 \pm 0.01	0.31 \pm 0.01	0.54 \pm 0.02	0.13 \pm 0.01	0.71 \pm 0.01
	Manipulated	75.56	0.99	0.30 \pm 0.01	0.26 \pm 0.01	0.67 \pm 0.03	0.12 \pm 0.00	0.61 \pm 0.02
8	Original	76.13	1.00	0.22 \pm 0.01	0.31 \pm 0.01	0.57 \pm 0.02	0.13 \pm 0.01	0.72 \pm 0.01
	Manipulated	75.49	1.00	0.31 \pm 0.01	0.26 \pm 0.01	0.68 \pm 0.03	0.13 \pm 0.01	0.60 \pm 0.01
9	Original	76.13	1.00	0.20 \pm 0.01	0.31 \pm 0.01	0.49 \pm 0.02	0.13 \pm 0.01	0.70 \pm 0.01
	Manipulated	75.46	1.00	0.29 \pm 0.02	0.26 \pm 0.02	0.65 \pm 0.04	0.12 \pm 0.00	0.61 \pm 0.02



Figure 14: Manipulating the first 10 output neurons in **ResNet-50** with GS. Manipulated FV examples consistently align with the target image.

D.5 Accuracy – Manipulation Trade-Off

We expand on the experimental results of the accuracy–manipulation trade-off analysis for the *Gradient Slingshots* attack, introduced in Sec. 4.2, with additional findings reported in Tables 17 to 21 and Figs. 15 to 18

Table 17: Accuracy–manipulation trade-off for the GS attack on the “zero” output neuron in **6-layer CNN** . Reported are test accuracy (in %), AUROC for the “zero” class, and the mean \pm standard deviation of alignment and similarity metrics, computed over 100 independent FV runs.

α	AUC	Acc.	Alignment		Target Similarity			
			Target Lbl. \uparrow	GT Lbl. \downarrow	CLIP \uparrow	MSE \downarrow	LPIPS \downarrow	SSIM \uparrow
Original	1.00	99.67	0.29 \pm 0.01	0.27 \pm 0.00	0.88 \pm 0.01	0.13 \pm 0.01	0.15 \pm 0.01	0.04 \pm 0.03
0.990	1.00	99.53	0.29 \pm 0.01	0.27 \pm 0.00	0.88 \pm 0.01	0.13 \pm 0.01	0.15 \pm 0.01	0.06 \pm 0.03
0.900	1.00	99.28	0.30 \pm 0.01	0.26 \pm 0.01	0.89 \pm 0.01	0.10 \pm 0.00	0.15 \pm 0.01	0.13 \pm 0.02
0.800	1.00	98.98	0.32 \pm 0.01	0.25 \pm 0.00	0.93 \pm 0.01	0.03 \pm 0.00	0.11 \pm 0.02	0.75 \pm 0.01
0.700	1.00	98.89	0.32 \pm 0.01	0.25 \pm 0.00	0.95 \pm 0.01	0.02 \pm 0.00	0.07 \pm 0.02	0.76 \pm 0.03
0.500	1.00	98.10	0.25 \pm 0.01	0.24 \pm 0.01	0.86 \pm 0.01	0.12 \pm 0.00	0.29 \pm 0.04	0.07 \pm 0.02
0.200	0.99	96.34	0.31 \pm 0.03	0.25 \pm 0.01	0.93 \pm 0.04	0.04 \pm 0.04	0.11 \pm 0.10	0.62 \pm 0.29
0.050	0.99	94.36	0.27 \pm 0.01	0.24 \pm 0.00	0.86 \pm 0.01	0.11 \pm 0.00	0.24 \pm 0.01	0.15 \pm 0.01
0.010	0.87	70.88	0.32 \pm 0.00	0.25 \pm 0.00	0.95 \pm 0.00	0.02 \pm 0.00	0.04 \pm 0.00	0.84 \pm 0.01
0.005	0.84	52.52	0.33 \pm 0.00	0.25 \pm 0.00	0.96 \pm 0.01	0.02 \pm 0.00	0.03 \pm 0.00	0.82 \pm 0.01
0.001	0.54	19.39	0.33 \pm 0.00	0.25 \pm 0.00	0.95 \pm 0.00	0.02 \pm 0.00	0.04 \pm 0.00	0.77 \pm 0.01

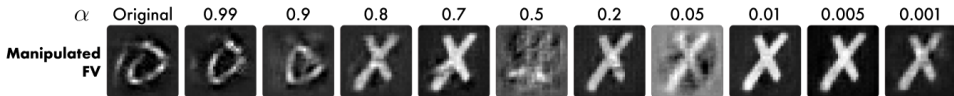


Figure 15: Sample FVs at different values of α for **6-layer CNN**.

Table 18: Accuracy–manipulation trade-off for the GS attack on the “cat” output neuron in **VGG9** . Reported are test accuracy (in %), AUROC for the “cat” class, and the mean \pm standard deviation of alignment and similarity metrics, computed over 100 independent FV runs.

α	AUC	Acc.	Alignment		Target Similarity			
			Target Lbl. \uparrow	GT Lbl. \downarrow	CLIP \uparrow	MSE \downarrow	LPIPS \downarrow	SSIM \uparrow
Original	0.97	86.33	0.24 \pm 0.01	0.29 \pm 0.01	0.74 \pm 0.02	0.08 \pm 0.00	0.25 \pm 0.02	0.03 \pm 0.02
0.9900	0.97	86.10	0.24 \pm 0.01	0.29 \pm 0.01	0.74 \pm 0.02	0.08 \pm 0.01	0.25 \pm 0.02	0.03 \pm 0.02
0.8000	0.97	87.20	0.24 \pm 0.01	0.29 \pm 0.01	0.73 \pm 0.03	0.09 \pm 0.01	0.26 \pm 0.02	0.02 \pm 0.02
0.5000	0.97	83.90	0.24 \pm 0.00	0.23 \pm 0.01	0.78 \pm 0.01	0.01 \pm 0.00	0.09 \pm 0.01	0.19 \pm 0.06
0.1000	0.97	86.40	0.23 \pm 0.01	0.24 \pm 0.01	0.77 \pm 0.02	0.01 \pm 0.00	0.14 \pm 0.02	0.25 \pm 0.05
0.0500	0.96	85.10	0.23 \pm 0.01	0.24 \pm 0.01	0.75 \pm 0.02	0.02 \pm 0.00	0.11 \pm 0.02	0.27 \pm 0.05
0.0250	0.96	85.15	0.24 \pm 0.00	0.24 \pm 0.01	0.78 \pm 0.01	0.02 \pm 0.00	0.16 \pm 0.02	0.33 \pm 0.04
0.0100	0.95	81.90	0.25 \pm 0.01	0.24 \pm 0.01	0.81 \pm 0.02	0.01 \pm 0.00	0.15 \pm 0.03	0.40 \pm 0.05
0.0050	0.94	82.20	0.30 \pm 0.04	0.23 \pm 0.01	0.87 \pm 0.04	0.01 \pm 0.00	0.08 \pm 0.02	0.51 \pm 0.05
0.0010	0.86	72.70	0.29 \pm 0.03	0.22 \pm 0.01	0.87 \pm 0.04	0.01 \pm 0.00	0.10 \pm 0.02	0.53 \pm 0.04
0.0001	0.54	9.50	0.24 \pm 0.01	0.24 \pm 0.01	0.80 \pm 0.01	0.02 \pm 0.00	0.14 \pm 0.02	0.30 \pm 0.05

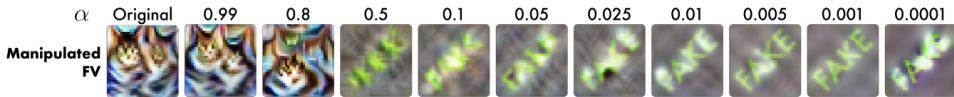


Figure 16: Sample FVs at different values of α for **VGG-9**.

Table 19: Accuracy–manipulation trade-off for the GS attack on the “gondola” output neuron in **ResNet-18**. Reported are test accuracy (in %), AUROC for the “gondola” class, and the mean \pm standard deviation of alignment and similarity metrics, computed over 100 independent FV runs.

α	AUC	Acc.	Alignment		Target Similarity			
			Target Lbl. \uparrow	GT Lbl. \downarrow	CLIP \uparrow	MSE \downarrow	LPIPS \downarrow	SSIM \uparrow
Original	0.99	71.89	0.21 \pm 0.01	0.25 \pm 0.02	0.64 \pm 0.03	0.09 \pm 0.01	0.59 \pm 0.04	0.03 \pm 0.02
0.999000	0.98	70.30	0.21 \pm 0.01	0.25 \pm 0.02	0.65 \pm 0.03	0.09 \pm 0.01	0.58 \pm 0.05	0.04 \pm 0.02
0.997000	0.97	69.50	0.24 \pm 0.02	0.24 \pm 0.02	0.73 \pm 0.03	0.07 \pm 0.01	0.35 \pm 0.04	0.06 \pm 0.03
0.995000	0.97	71.40	0.25 \pm 0.02	0.24 \pm 0.02	0.75 \pm 0.03	0.07 \pm 0.01	0.34 \pm 0.06	0.07 \pm 0.03
0.993000	0.96	68.40	0.24 \pm 0.02	0.23 \pm 0.02	0.74 \pm 0.03	0.07 \pm 0.01	0.41 \pm 0.06	0.07 \pm 0.03
0.990000	0.94	69.30	0.24 \pm 0.02	0.22 \pm 0.02	0.73 \pm 0.03	0.07 \pm 0.01	0.42 \pm 0.07	0.07 \pm 0.02
0.950000	0.87	39.10	0.22 \pm 0.01	0.18 \pm 0.01	0.69 \pm 0.03	0.10 \pm 0.01	0.58 \pm 0.04	0.04 \pm 0.02
0.900000	0.79	11.00	0.23 \pm 0.01	0.19 \pm 0.01	0.70 \pm 0.02	0.08 \pm 0.01	0.57 \pm 0.03	0.09 \pm 0.03
0.500000	0.63	0.60	0.23 \pm 0.01	0.20 \pm 0.01	0.61 \pm 0.03	0.15 \pm 0.01	0.50 \pm 0.03	0.03 \pm 0.02
0.100000	0.51	0.80	0.22 \pm 0.01	0.18 \pm 0.02	0.68 \pm 0.03	0.09 \pm 0.03	0.63 \pm 0.14	0.10 \pm 0.02



Figure 17: Sample FVs at different values of α for **ResNet-18**.

Table 20: Accuracy–manipulation trade-off for the GS attack on the “wolf spider” output neuron in **ResNet-50**. Extended version of Table 1 including additional α values and similarity metrics.

α	AUC	Acc.	Alignment		Target Similarity			
			Target Lbl. \uparrow	GT Lbl. \downarrow	CLIP \uparrow	MSE \downarrow	LPIPS \downarrow	SSIM \uparrow
Original	1.00	76.13	0.23 \pm 0.01	0.29 \pm 0.02	0.53 \pm 0.02	0.12 \pm 0.01	0.69 \pm 0.01	0.05 \pm 0.01
0.90	1.00	76.07	0.22 \pm 0.01	0.28 \pm 0.02	0.53 \pm 0.02	0.12 \pm 0.01	0.69 \pm 0.01	0.05 \pm 0.01
0.80	1.00	76.00	0.22 \pm 0.01	0.28 \pm 0.02	0.52 \pm 0.02	0.13 \pm 0.01	0.68 \pm 0.01	0.05 \pm 0.01
0.70	1.00	75.77	0.23 \pm 0.02	0.27 \pm 0.02	0.53 \pm 0.03	0.12 \pm 0.01	0.67 \pm 0.02	0.05 \pm 0.01
0.64	1.00	75.13	0.31 \pm 0.01	0.23 \pm 0.01	0.69 \pm 0.02	0.12 \pm 0.01	0.59 \pm 0.02	0.04 \pm 0.01
0.62	1.00	74.83	0.32 \pm 0.01	0.23 \pm 0.01	0.68 \pm 0.02	0.12 \pm 0.00	0.59 \pm 0.02	0.04 \pm 0.01
0.60	1.00	74.51	0.32 \pm 0.01	0.23 \pm 0.01	0.69 \pm 0.02	0.12 \pm 0.00	0.60 \pm 0.02	0.04 \pm 0.01
0.58	1.00	74.45	0.32 \pm 0.01	0.23 \pm 0.01	0.69 \pm 0.02	0.12 \pm 0.01	0.60 \pm 0.02	0.04 \pm 0.01
0.56	1.00	73.67	0.32 \pm 0.01	0.22 \pm 0.01	0.70 \pm 0.02	0.11 \pm 0.00	0.61 \pm 0.01	0.04 \pm 0.01
0.50	1.00	71.52	0.32 \pm 0.01	0.23 \pm 0.01	0.72 \pm 0.02	0.11 \pm 0.00	0.63 \pm 0.02	0.05 \pm 0.01
0.40	1.00	66.58	0.31 \pm 0.01	0.24 \pm 0.01	0.66 \pm 0.03	0.12 \pm 0.01	0.66 \pm 0.01	0.05 \pm 0.01
0.30	0.99	52.09	0.31 \pm 0.01	0.24 \pm 0.01	0.65 \pm 0.03	0.13 \pm 0.01	0.65 \pm 0.02	0.06 \pm 0.01
0.20	0.97	21.97	0.29 \pm 0.01	0.22 \pm 0.01	0.60 \pm 0.03	0.11 \pm 0.01	0.69 \pm 0.01	0.08 \pm 0.01
0.10	0.90	30.19	0.29 \pm 0.01	0.24 \pm 0.01	0.59 \pm 0.02	0.10 \pm 0.00	0.71 \pm 0.02	0.08 \pm 0.02
0.05	0.64	0.21	0.27 \pm 0.01	0.22 \pm 0.01	0.54 \pm 0.01	0.09 \pm 0.00	0.76 \pm 0.02	0.11 \pm 0.01
0.01	0.61	0.14	0.26 \pm 0.00	0.24 \pm 0.01	0.53 \pm 0.01	0.09 \pm 0.00	0.78 \pm 0.01	0.07 \pm 0.00

Table 21: Accuracy–manipulation trade-off for the GS attack on the “broccoli” output neuron in **ViT-L/32**. Reported are test accuracy (in %), AUROC for the “broccoli” class, and the mean \pm standard deviation of alignment and similarity metrics, computed over 100 independent FV runs.

α	AUC	Acc.	Alignment		Target Similarity			
			Target Lbl. \uparrow	GT Lbl. \downarrow	CLIP \uparrow	MSE \downarrow	LPIPS \downarrow	SSIM \uparrow
Original	1.00	76.97	0.23 \pm 0.02	0.28 \pm 0.02	0.51 \pm 0.02	0.08 \pm 0.00	0.73 \pm 0.03	0.08 \pm 0.01
0.999999	1.00	76.58	0.22 \pm 0.02	0.28 \pm 0.02	0.51 \pm 0.02	0.08 \pm 0.00	0.73 \pm 0.03	0.08 \pm 0.01
0.999900	1.00	76.64	0.29 \pm 0.03	0.27 \pm 0.03	0.53 \pm 0.03	0.09 \pm 0.00	0.74 \pm 0.04	0.08 \pm 0.01
0.999500	0.99	76.06	0.29 \pm 0.02	0.25 \pm 0.01	0.50 \pm 0.02	0.07 \pm 0.00	0.74 \pm 0.02	0.08 \pm 0.01
0.999000	0.99	75.96	0.28 \pm 0.02	0.25 \pm 0.01	0.49 \pm 0.02	0.07 \pm 0.00	0.72 \pm 0.02	0.09 \pm 0.01
0.990000	0.99	72.42	0.29 \pm 0.02	0.25 \pm 0.01	0.49 \pm 0.02	0.06 \pm 0.00	0.71 \pm 0.01	0.11 \pm 0.01
0.100000	0.50	0.10	0.25 \pm 0.01	0.27 \pm 0.01	0.49 \pm 0.01	0.05 \pm 0.00	0.75 \pm 0.01	0.18 \pm 0.01



Figure 18: Sample FVs at different values of α for ViT-L/32.

D.6 Impact of Target Image on Manipulation

We provide additional quantitative evaluation of the effect of the target image on manipulation success, extending the results from Sec. 4.4 to an additional set of target images, shown in Fig. 19.

Target source	Hold-out samples		
	K	L	M
Target image			
Manipulated FV			
Δ Accuracy, %	-2.29	-1.79	-4.39
Dist. to target ↓	0.48±0.03	0.31±0.02	0.52±0.10

Figure 19: Manipulation results for different target images by source. Extended version of Table 13 including additional target images.

D.7 Attack Detection

We provide additional qualitative results for our attack detection scheme in Fig. 20, extending the evaluation described in Sec. 6 to additional experimental settings.

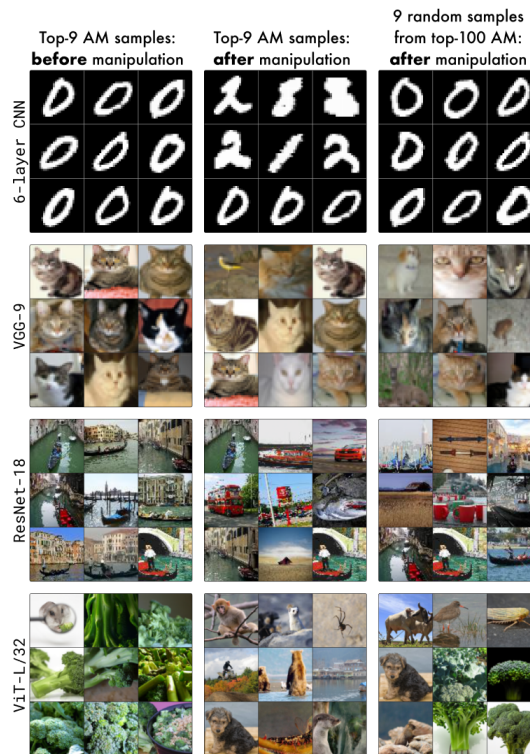


Figure 20: Top-9 most activating test samples before and after the GS attack. While the attack can substantially change which samples rank as the most activating across a dataset, broader sampling from the top of the AM distribution often recovers the original concept.

NeurIPS Paper Checklist

1. Claims

Question: Do the main claims made in the abstract and introduction accurately reflect the paper's contributions and scope?

Answer: [Yes]

Justification: We demonstrate in Sec. 4 and Sec. 5, with additional results in the Appendix, that:

- (a) Our method can “conceal the true functionality of arbitrary neurons by replacing their original explanations with selected target explanations”. We support this by visualizing Feature Visualizations (FVs) from manipulated models and quantitatively measuring their similarity to the target image.
- (b) This manipulation largely “preserves the model’s external behavior and internal mechanisms”, as demonstrated by the relatively small changes to the classification accuracy and the AUROC scores of the target features in various settings.

Guidelines:

- The answer NA means that the abstract and introduction do not include the claims made in the paper.
- The abstract and/or introduction should clearly state the claims made, including the contributions made in the paper and important assumptions and limitations. A No or NA answer to this question will not be perceived well by the reviewers.
- The claims made should match theoretical and experimental results, and reflect how much the results can be expected to generalize to other settings.
- It is fine to include aspirational goals as motivation as long as it is clear that these goals are not attained by the paper.

2. Limitations

Question: Does the paper discuss the limitations of the work performed by the authors?

Answer: [Yes]

Justification: The limitations are discussed in Sec. 7.

Guidelines:

- The answer NA means that the paper has no limitation while the answer No means that the paper has limitations, but those are not discussed in the paper.
- The authors are encouraged to create a separate "Limitations" section in their paper.
- The paper should point out any strong assumptions and how robust the results are to violations of these assumptions (e.g., independence assumptions, noiseless settings, model well-specification, asymptotic approximations only holding locally). The authors should reflect on how these assumptions might be violated in practice and what the implications would be.
- The authors should reflect on the scope of the claims made, e.g., if the approach was only tested on a few datasets or with a few runs. In general, empirical results often depend on implicit assumptions, which should be articulated.
- The authors should reflect on the factors that influence the performance of the approach. For example, a facial recognition algorithm may perform poorly when image resolution is low or images are taken in low lighting. Or a speech-to-text system might not be used reliably to provide closed captions for online lectures because it fails to handle technical jargon.
- The authors should discuss the computational efficiency of the proposed algorithms and how they scale with dataset size.
- If applicable, the authors should discuss possible limitations of their approach to address problems of privacy and fairness.
- While the authors might fear that complete honesty about limitations might be used by reviewers as grounds for rejection, a worse outcome might be that reviewers discover limitations that aren't acknowledged in the paper. The authors should use their best

judgment and recognize that individual actions in favor of transparency play an important role in developing norms that preserve the integrity of the community. Reviewers will be specifically instructed to not penalize honesty concerning limitations.

3. Theory assumptions and proofs

Question: For each theoretical result, does the paper provide the full set of assumptions and a complete (and correct) proof?

Answer: [Yes]

Justification: To establish the theoretical possibility of our attack, we provide a formal proof, along with its assumptions, in Sec. 3.1.

Guidelines:

- The answer NA means that the paper does not include theoretical results.
- All the theorems, formulas, and proofs in the paper should be numbered and cross-referenced.
- All assumptions should be clearly stated or referenced in the statement of any theorems.
- The proofs can either appear in the main paper or the supplemental material, but if they appear in the supplemental material, the authors are encouraged to provide a short proof sketch to provide intuition.
- Inversely, any informal proof provided in the core of the paper should be complemented by formal proofs provided in appendix or supplemental material.
- Theorems and Lemmas that the proof relies upon should be properly referenced.

4. Experimental result reproducibility

Question: Does the paper fully disclose all the information needed to reproduce the main experimental results of the paper to the extent that it affects the main claims and/or conclusions of the paper (regardless of whether the code and data are provided or not)?

Answer: [Yes]

Justification: The experimental details necessary to reproduce our results, including our algorithm, the datasets, models, methods, metrics, and parameters we use, are provided throughout the main text and in the Appendix.

Guidelines:

- The answer NA means that the paper does not include experiments.
- If the paper includes experiments, a No answer to this question will not be perceived well by the reviewers: Making the paper reproducible is important, regardless of whether the code and data are provided or not.
- If the contribution is a dataset and/or model, the authors should describe the steps taken to make their results reproducible or verifiable.
- Depending on the contribution, reproducibility can be accomplished in various ways. For example, if the contribution is a novel architecture, describing the architecture fully might suffice, or if the contribution is a specific model and empirical evaluation, it may be necessary to either make it possible for others to replicate the model with the same dataset, or provide access to the model. In general, releasing code and data is often one good way to accomplish this, but reproducibility can also be provided via detailed instructions for how to replicate the results, access to a hosted model (e.g., in the case of a large language model), releasing of a model checkpoint, or other means that are appropriate to the research performed.
- While NeurIPS does not require releasing code, the conference does require all submissions to provide some reasonable avenue for reproducibility, which may depend on the nature of the contribution. For example
 - (a) If the contribution is primarily a new algorithm, the paper should make it clear how to reproduce that algorithm.
 - (b) If the contribution is primarily a new model architecture, the paper should describe the architecture clearly and fully.

- (c) If the contribution is a new model (e.g., a large language model), then there should either be a way to access this model for reproducing the results or a way to reproduce the model (e.g., with an open-source dataset or instructions for how to construct the dataset).
- (d) We recognize that reproducibility may be tricky in some cases, in which case authors are welcome to describe the particular way they provide for reproducibility. In the case of closed-source models, it may be that access to the model is limited in some way (e.g., to registered users), but it should be possible for other researchers to have some path to reproducing or verifying the results.

5. Open access to data and code

Question: Does the paper provide open access to the data and code, with sufficient instructions to faithfully reproduce the main experimental results, as described in supplemental material?

Answer: [\[Yes\]](#)

Justification: We provide the code in the supplementary materials, and use publicly available models, datasets and methods.

Guidelines:

- The answer NA means that paper does not include experiments requiring code.
- Please see the NeurIPS code and data submission guidelines (<https://nips.cc/public/guides/CodeSubmissionPolicy>) for more details.
- While we encourage the release of code and data, we understand that this might not be possible, so “No” is an acceptable answer. Papers cannot be rejected simply for not including code, unless this is central to the contribution (e.g., for a new open-source benchmark).
- The instructions should contain the exact command and environment needed to reproduce the results. See the NeurIPS code and data submission guidelines (<https://nips.cc/public/guides/CodeSubmissionPolicy>) for more details.
- The authors should provide instructions on data access and preparation, including how to access the raw data, preprocessed data, intermediate data, and generated data, etc.
- The authors should provide scripts to reproduce all experimental results for the new proposed method and baselines. If only a subset of experiments are reproducible, they should state which ones are omitted from the script and why.
- At submission time, to preserve anonymity, the authors should release anonymized versions (if applicable).
- Providing as much information as possible in supplemental material (appended to the paper) is recommended, but including URLs to data and code is permitted.

6. Experimental setting/details

Question: Does the paper specify all the training and test details (e.g., data splits, hyperparameters, how they were chosen, type of optimizer, etc.) necessary to understand the results?

Answer: [\[Yes\]](#)

Justification: We specify and justify the training and test details, including dataset splits, hyperparameters, and optimizer types, primarily in the Appendix.

Guidelines:

- The answer NA means that the paper does not include experiments.
- The experimental setting should be presented in the core of the paper to a level of detail that is necessary to appreciate the results and make sense of them.
- The full details can be provided either with the code, in appendix, or as supplemental material.

7. Experiment statistical significance

Question: Does the paper report error bars suitably and correctly defined or other appropriate information about the statistical significance of the experiments?

Answer: [Yes]

Justification: We report standard deviations for similarity metrics between target images and manipulated FVs in Sec. 4 and Sec. 5, and include them in the experimental results in the Appendix.

Guidelines:

- The answer NA means that the paper does not include experiments.
- The authors should answer "Yes" if the results are accompanied by error bars, confidence intervals, or statistical significance tests, at least for the experiments that support the main claims of the paper.
- The factors of variability that the error bars are capturing should be clearly stated (for example, train/test split, initialization, random drawing of some parameter, or overall run with given experimental conditions).
- The method for calculating the error bars should be explained (closed form formula, call to a library function, bootstrap, etc.)
- The assumptions made should be given (e.g., Normally distributed errors).
- It should be clear whether the error bar is the standard deviation or the standard error of the mean.
- It is OK to report 1-sigma error bars, but one should state it. The authors should preferably report a 2-sigma error bar than state that they have a 96% CI, if the hypothesis of Normality of errors is not verified.
- For asymmetric distributions, the authors should be careful not to show in tables or figures symmetric error bars that would yield results that are out of range (e.g. negative error rates).
- If error bars are reported in tables or plots, The authors should explain in the text how they were calculated and reference the corresponding figures or tables in the text.

8. Experiments compute resources

Question: For each experiment, does the paper provide sufficient information on the computer resources (type of compute workers, memory, time of execution) needed to reproduce the experiments?

Answer: [Yes]

Justification: The computational resources are detailed in the Appendix.

Guidelines:

- The answer NA means that the paper does not include experiments.
- The paper should indicate the type of compute workers CPU or GPU, internal cluster, or cloud provider, including relevant memory and storage.
- The paper should provide the amount of compute required for each of the individual experimental runs as well as estimate the total compute.
- The paper should disclose whether the full research project required more compute than the experiments reported in the paper (e.g., preliminary or failed experiments that didn't make it into the paper).

9. Code of ethics

Question: Does the research conducted in the paper conform, in every respect, with the NeurIPS Code of Ethics <https://neurips.cc/public/EthicsGuidelines>?

Answer: [Yes]

Justification: This paper complies with the NeurIPS Code of Ethics.

Guidelines:

- The answer NA means that the authors have not reviewed the NeurIPS Code of Ethics.
- If the authors answer No, they should explain the special circumstances that require a deviation from the Code of Ethics.
- The authors should make sure to preserve anonymity (e.g., if there is a special consideration due to laws or regulations in their jurisdiction).

10. Broader impacts

Question: Does the paper discuss both potential positive societal impacts and negative societal impacts of the work performed?

Answer: [Yes]

Justification: The potential societal impact is described in Sec. 7.

Guidelines:

- The answer NA means that there is no societal impact of the work performed.
- If the authors answer NA or No, they should explain why their work has no societal impact or why the paper does not address societal impact.
- Examples of negative societal impacts include potential malicious or unintended uses (e.g., disinformation, generating fake profiles, surveillance), fairness considerations (e.g., deployment of technologies that could make decisions that unfairly impact specific groups), privacy considerations, and security considerations.
- The conference expects that many papers will be foundational research and not tied to particular applications, let alone deployments. However, if there is a direct path to any negative applications, the authors should point it out. For example, it is legitimate to point out that an improvement in the quality of generative models could be used to generate deepfakes for disinformation. On the other hand, it is not needed to point out that a generic algorithm for optimizing neural networks could enable people to train models that generate Deepfakes faster.
- The authors should consider possible harms that could arise when the technology is being used as intended and functioning correctly, harms that could arise when the technology is being used as intended but gives incorrect results, and harms following from (intentional or unintentional) misuse of the technology.
- If there are negative societal impacts, the authors could also discuss possible mitigation strategies (e.g., gated release of models, providing defenses in addition to attacks, mechanisms for monitoring misuse, mechanisms to monitor how a system learns from feedback over time, improving the efficiency and accessibility of ML).

11. Safeguards

Question: Does the paper describe safeguards that have been put in place for responsible release of data or models that have a high risk for misuse (e.g., pretrained language models, image generators, or scraped datasets)?

Answer: [NA]

Justification: This paper is not accompanied by the release of data or models.

Guidelines:

- The answer NA means that the paper poses no such risks.
- Released models that have a high risk for misuse or dual-use should be released with necessary safeguards to allow for controlled use of the model, for example by requiring that users adhere to usage guidelines or restrictions to access the model or implementing safety filters.
- Datasets that have been scraped from the Internet could pose safety risks. The authors should describe how they avoided releasing unsafe images.
- We recognize that providing effective safeguards is challenging, and many papers do not require this, but we encourage authors to take this into account and make a best faith effort.

12. Licenses for existing assets

Question: Are the creators or original owners of assets (e.g., code, data, models), used in the paper, properly credited and are the license and terms of use explicitly mentioned and properly respected?

Answer: [Yes]

Justification: The license terms of use are fully respected, with details and attributions listed in the Appendix.

Guidelines:

- The answer NA means that the paper does not use existing assets.
- The authors should cite the original paper that produced the code package or dataset.
- The authors should state which version of the asset is used and, if possible, include a URL.
- The name of the license (e.g., CC-BY 4.0) should be included for each asset.
- For scraped data from a particular source (e.g., website), the copyright and terms of service of that source should be provided.
- If assets are released, the license, copyright information, and terms of use in the package should be provided. For popular datasets, paperswithcode.com/datasets has curated licenses for some datasets. Their licensing guide can help determine the license of a dataset.
- For existing datasets that are re-packaged, both the original license and the license of the derived asset (if it has changed) should be provided.
- If this information is not available online, the authors are encouraged to reach out to the asset's creators.

13. New assets

Question: Are new assets introduced in the paper well documented and is the documentation provided alongside the assets?

Answer: [Yes]

Justification: We provided our code and use publicly available models, datasets and methods.

Guidelines:

- The answer NA means that the paper does not release new assets.
- Researchers should communicate the details of the dataset/code/model as part of their submissions via structured templates. This includes details about training, license, limitations, etc.
- The paper should discuss whether and how consent was obtained from people whose asset is used.
- At submission time, remember to anonymize your assets (if applicable). You can either create an anonymized URL or include an anonymized zip file.

14. Crowdsourcing and research with human subjects

Question: For crowdsourcing experiments and research with human subjects, does the paper include the full text of instructions given to participants and screenshots, if applicable, as well as details about compensation (if any)?

Answer: [NA]

Justification: This paper does not involve crowdsourcing and research with human subjects.

Guidelines:

- The answer NA means that the paper does not involve crowdsourcing nor research with human subjects.
- Including this information in the supplemental material is fine, but if the main contribution of the paper involves human subjects, then as much detail as possible should be included in the main paper.
- According to the NeurIPS Code of Ethics, workers involved in data collection, curation, or other labor should be paid at least the minimum wage in the country of the data collector.

15. Institutional review board (IRB) approvals or equivalent for research with human subjects

Question: Does the paper describe potential risks incurred by study participants, whether such risks were disclosed to the subjects, and whether Institutional Review Board (IRB) approvals (or an equivalent approval/review based on the requirements of your country or institution) were obtained?

Answer: [NA]

Justification: This paper does not involve crowdsourcing and research with human subjects.

Guidelines:

- The answer NA means that the paper does not involve crowdsourcing nor research with human subjects.
- Depending on the country in which research is conducted, IRB approval (or equivalent) may be required for any human subjects research. If you obtained IRB approval, you should clearly state this in the paper.
- We recognize that the procedures for this may vary significantly between institutions and locations, and we expect authors to adhere to the NeurIPS Code of Ethics and the guidelines for their institution.
- For initial submissions, do not include any information that would break anonymity (if applicable), such as the institution conducting the review.

16. **Declaration of LLM usage**

Question: Does the paper describe the usage of LLMs if it is an important, original, or non-standard component of the core methods in this research? Note that if the LLM is used only for writing, editing, or formatting purposes and does not impact the core methodology, scientific rigorousness, or originality of the research, declaration is not required.

Answer: [NA]

Justification: This paper uses LLMs for text editing.

Guidelines:

- The answer NA means that the core method development in this research does not involve LLMs as any important, original, or non-standard components.
- Please refer to our LLM policy (<https://neurips.cc/Conferences/2025/LLM>) for what should or should not be described.